Visualization of Bacteria in a Contaminant Plume

Teresa A. Nowicki

Submitted in partial fulfillment
of the requirements for the degree of
Master of Science in Hydrology

New Mexico Institute of Mining and Technology

I. Acknowledgments

I would like to acknowledge the U.S. Department of Energy Subsurface Science Program, Office of Health and Environmental Research, for funding this project. I would also like to acknowledge my advisor, John Wilson, and my other committee members Rob Bowman and Tom Kieft.

I thank those who helped me with my experiments, including Monty Flinsch for helping with sampling, Jiamin Wan for technical advice and Paul Hofmann for building the box. Thanks also go to Eric Seagren at Northwestern University for giving me the information I needed and keeping me up to date on his work.

I would like to thank my friends who helped me get through the years here, including, in alphabetical order, Robin Brown, the Burkes, Jinfang He, Daphne Neel, Tracy Roth, Janet Sorrentino, Ellen Wilch and Shawn and Alice. I would also like to thank my family members who made it possible for me to be here: Mom and Steve, Dad and Shirley and my brother Mark, who always came through when asked.

Finally, I would like to thank my husband, E. David Grenham, without whom I would never have come here and without whom I would probably have gone insane.

II.Table of Contents

III. List of Tables

IV. List of Figures

V. Abstract

Bacteria can degrade many common contaminants such as gasoline components. These hydrocarbons may be toxic at high concentrations. Bioremediation models make assumptions about the distribution of bacteria in the subsurface. The distribution of bacteria depends on many factors, including nutrient supply. Bacteria will be situated near a nutrient source; however, if the source is toxic in high concentrations, the cells may locate at some distance where the concentration is lower.

An experiment was designed to test the hypothesis that the bacteria will situate in a portion of a toluene plume where the concentrations are high enough to act as a nutrient supply but not so high as to be toxic.

It was discovered that the bacteria colonized close to the contaminant source. They were close enough that one would expect the dissolved toluene concentrations to be toxic. One possible explanation for their proximity to the contaminant source is that there was an extracellular polysaccharide coating that lowered toluene concentrations at the cell wall. Another interpretation may be that the bacteria were able to adapt to high toluene concentrations.

VI. Introduction

Bioremediation modeling tends to focus on contaminant degradation rates rather than dynamics of growth and decay (Harvey and Widdowson, 1992). In all models, assumptions are made about the growth rate of the bacteria and their subsurface distribution. In most models, the initial distribution of the bacteria is assumed to be uniform and attached to solids. The actual distribution is heterogeneous and is a function of chemical, physical and physiochemical environmental factors (Yanagita, 1990). Among the physical factors is the presence of interfaces, either liquid-liquid or solid-liquid. Bacteria exist both as free-living and attached cells, but it is predominantly the attached cells that degrade contaminants (Ellwood et al., 1979). Nutrient supply is the main chemical factor. Nutrients such as a carbon source (e.g., a hydrocarbon) and an electron acceptor are the basic needs of heterotrophic bacteria, but other minerals may also be needed. In order for the bacteria to remediate the contaminant, the chemical must act as a nutrient for the cells or must be cometabolized with some other nutrient. Another nutrient that may be required is oxygen, which acts as a terminal electron acceptor. Many models describe degradation of a contaminant with oxygen as a limiting nutrient (e.g., Molz et al., 1986, MacQuarrie et al., 1990, Borden and Bedient, 1986).

If this contaminant is a non-aqueous phase liquid (NAPL), it can exist as a blob in the saturated zone, a pool above or below the saturated zone or dissolved in the aqueous phase. Bacteria degrade contaminants after they have dissolved out of a pool or blob and into the water. Contaminant concentration profiles for the aqueous phase in subsurface systems are highly dependent on flow rates and NAPL saturation distributions (Miller et al., 1990; Conrad et al., 1992). Among the characteristics of contaminant saturation that are important are blob shape and size and lateral dimensions of the exposure zone (Powers et al., 1991). These characteristics have an effect on NAPL remediation by flushing or biodegradation because for either remediation effort to succeed the contaminant must dissolve out of the pool or blob.

Working in conjunction with Bruce Rittmannn and Eric Seagren at the University of Illinois (both now at Northwestern University), we experimentally investigated bacterial growth in the vicinity of a NAPL pool for a contaminant that can act as a nutrient but is inhibitory at higher concentrations. Experiments and modeling were performed with toluene, a common hydrocarbon NAPL that is self-inhibitory (see appendix A). The fundamental hypothesis of the research is that *in situ* biodegradation of the dissolved NAPL components can serve as a significant sink term for the solute and can cause an increase in the concentration gradient in the aqueous phase, resulting in an increase in NAPL pool dissolution above that produced by flushing alone (Seagren et al., 1993; Seagren et al., 1994). Using a pure culture of *Pseudomonas putida*, a toluene degrading bacterium, Seagren and Rittmannn experimentally demonstrated the phenomenon of bioenhanced toluene dissolution, with the degree of enhancement dependent upon the experimental conditions (Seagren, 1994). In experiments with low interfacial toluene equilibrium concentrations, a significant amount of bioenhanced toluene pool dissolution occurred. The interfacial toluene equilibrium concentration is the aqueous phase toluene concentration as calculated from a local equilibrium model of the system. Where the interfacial toluene equilibrium concentrations were higher, biologically mediated enhanced dissolution was either not observed or was statistically insignificant. Toluene concentrations were varied by changing the fraction of toluene in a toluene-dodecane pool. Measurements of the biomass accumulation and modeling analyses suggested that the high concentrations caused a toxicity effect that was responsible for the observed variation. This effect caused a decrease in measured biomass directly below the pool and a spreading out of the bacteria.

For the bacteria to increase the toluene pool dissolution effectively, this toxicity effect must be mitigated. Using this observation as a starting point, we developed the hypothesis that the bacteria will colonize a boundary-layer region along the contaminant plume where the toluene's concentration is favorable to their growth. This is illustrated

for the geometry of Seagren and Rittmannn's experiment in figure 1. In this region, concentrations will be high enough that the bacteria can use the contaminant as a food source, but it will be low enough that the chemical is not toxic. The spatial distribution of bacteria controls the remediation effect. The actively degrading cells closest to the NAPL will have the greatest impact on the contaminant, increasing dissolution rates through increased chemical gradients. If the bacteria are too far from the NAPL source, their influence on dissolution will be small, as may have occurred in Seagren and Rittmannn's experiment.

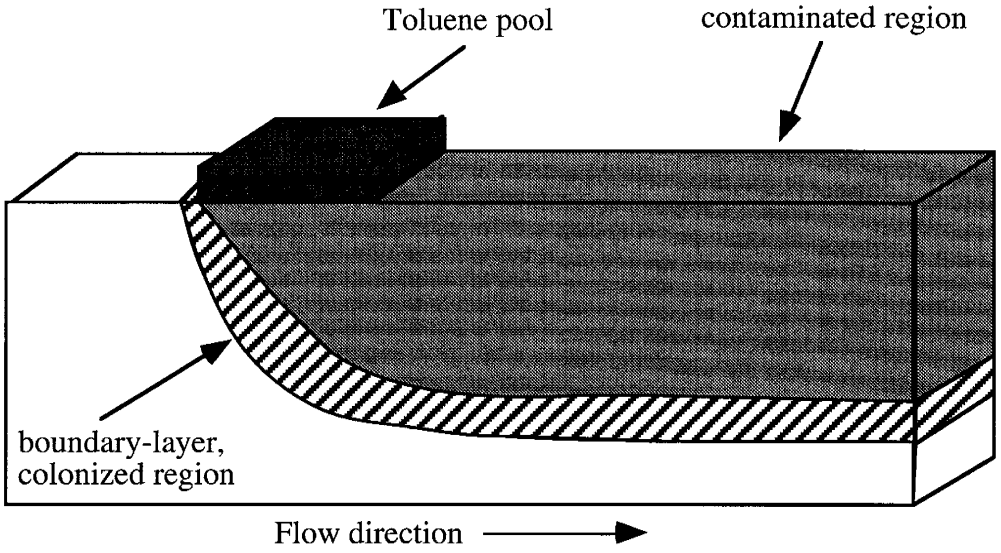

Figure 1 Hypothetical bacterial distribution in a contaminant plume.
In this schematic, the bacteria have colonized and are actively degrading the contaminant in the boundary-layer.

We designed a micromodel pattern that mimicked a cross-section of the column used at the University of Illinois. Micromodels are transparent pore networks created by etching a pattern onto two glass plates which are then fused (Conrad et al., 1992; Wan and Wilson, 1994b; Wan et al., 1994). The pores have complex three-dimensional structure but are part of a two-dimensional network that allows direct visualization of the components -- bacteria, solid, fluid phases -- under investigation. Using the micromodel,

we were able to examine the spatial and temporal distribution of the bacteria in a toluene plume, consequently testing the boundary-layer theory. Figure 2 shows how the hypothetical boundary-layer bacterial distribution in a column experiment (e.g., figure 1) would translate to a micromodel with a hexagonal pore network.

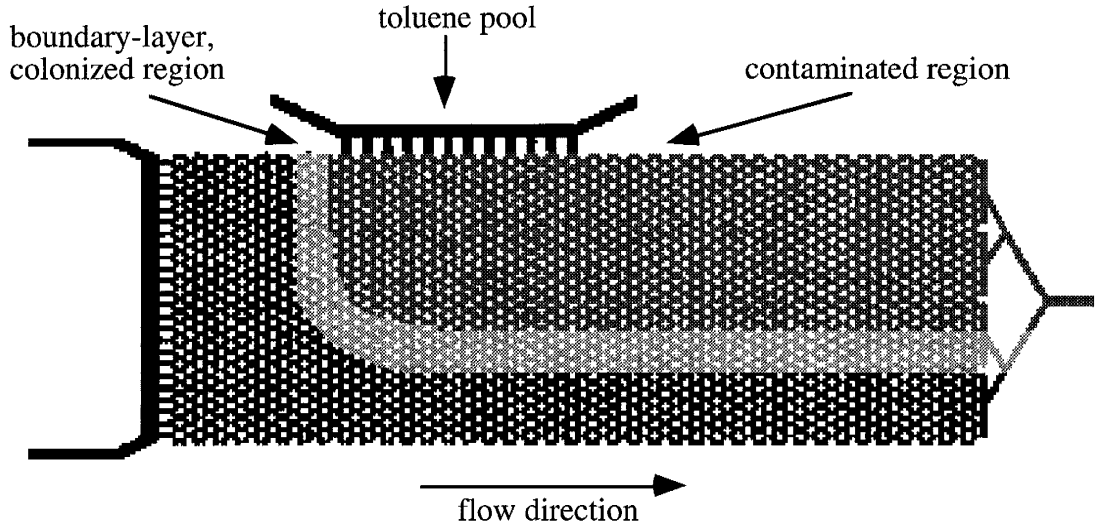

Figure 2 Hypothetical bacterial distribution in a micromodel.

VII. Experimental Design and Methods

The experiment was designed to determine the position of bacteria in a contaminant plume, through mimicking the experiment run at the University of Illinois by Seagren under Rittmannn (Seagren, 1994). We chose to use a similar design where the hexagonal network was scaled 1:1 to the size of the glass beads in their box. We also designed our model to have the same depth and same size NAPL source, but due to fabrication constraints our model was shorter, as shown in figure 3. We used the same bacteria and growth medium and wherever possible the same procedures, such as the order of introducing bacteria and contaminant.

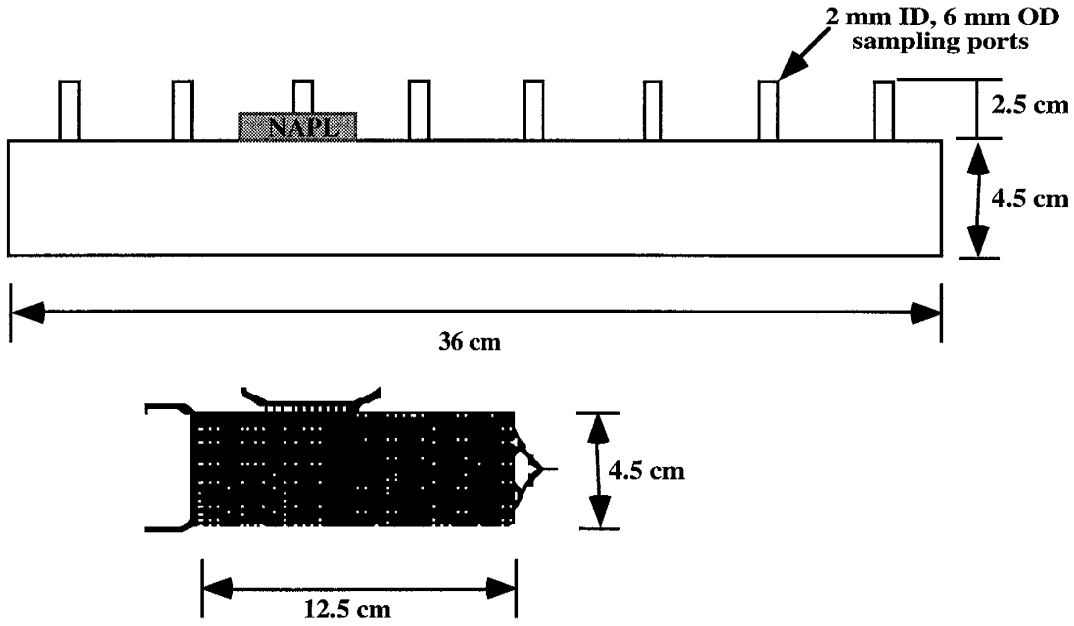

Figure 3 Design of the column and micromodel used in the experiments. The top object is a schematic of the box that was used at the University of Illinois for their NAPL-dissolution experiments (Seagren, 1994). The bottom object is the micromodel pattern designed to mimic their box. The pattern has lost much of its detail in reducing it to the same pictorial scale as the column.

The micromodel experiment was set up with two controls and one test. The first control was a dissolution experiment. This was run without any particles or bacteria in the model. The second control was run with polystyrene latex colloidal sized particles and

was designed to determine whether the surface chemistry would determine the bacterial distribution. The colloids were selected to match the bacteria's hydrophobicity as measured by contact angle. The final test was conducted with fluorescently stained bacteria. By visualizing these bacteria, we could literally see if the hypothesis of bacteria colonizing the boundary-layer region is reasonable. We also measured toluene concentrations in the outflow to check that the bacteria were affecting concentrations and to better correlate our work with the University of Illinois work. The set of experiments was repeated three times in three individual micromodels, for a total of nine experiments.

A. Bacteria

Pseudomonas putida PpG9 was isolated from soil. We received cultures from the culture collection of I.C. Gunsalus at the University of Illinois, Urbana-Champaign. This strain carries the TOL plasmid and can degrade aromatic hydrocarbons. Bacteria with the TOL plasmid can grow on toluene, although toluene concentrations above 100 mg/l are inhibitory (Alvarez et al., 1991). *P. putida* was maintained on tryptic soy agar and broth (Difco). A second culture was maintained on mineral medium agar with toluene vapors. Prior to inoculation into the model, the bacteria were grown in mineral medium broth, see Table 1, (Seagren, 1994) with toluene vapors for 24 hours as in Seagren and Rittmann's experiment. The mineral medium broth was inoculated with bacteria from the second culture. The ionic strength of the liquid mineral medium was 0.086 M.

Table 1 Composition of mineral medium.

Mineral Medium	
Compound	g/L
KH_2PO_4	2.04
Na_2HPO_4	2.13
$(NH_4)_2SO_4$	1.0
$CaCl_2 \cdot 2H_2O$	0.0110
$MgSO_4 \cdot 7H_2O$	0.20
$FeSO_4 \cdot 7H_2O$	0.007
$ZnSO_4 \cdot H_2O$	0.002
$MnSO_4 \cdot H_2O$	0.00154
$CuCl_2$	0.00021
$CoCl_2 \cdot 6H_2O$	0.000404
H_3BO_3	0.00011
$Na_2MoO_4 \cdot 2H_2O$	0.00025
H_2SO_4 (conc.)	few drops to pH=6.8

The contact angles were measured using the thick smear technique of Aaron Mills of the University of Virginia (personal communication, Nov. 1992). *Pseudomonas putida* PpG9 were grown in mineral medium broth with toluene vapor until the suspension was very turbid (approximately 72 h). The suspension was then washed in artificial groundwater (AGW), see Table 2, and resuspended in AGW for 24 - 48 hours. The cells were then centrifuged at 12,100 x g for 10 minutes. The supernatant was removed and the centrifuge tube was placed on its side with the pellet facing up, so as not to rewet the pellet. A sterile inoculating loop was then used to smear the bacteria thickly onto a clean glass slide. This smear was allowed to dry in a desiccator for approximately 4 hours, and contact angle measurements were then made. The smear was not allowed to dry to cracking. A single drop of distilled water was placed on the smear with a nanoliter pipette. Measurements were made on both sides of the drop. Measurements were made in several spots on each smear using a Zeiss stereoscope with a goniometer eyepiece.

Table 2 Composition of AGW

AGW	
$1.5x10^{-5}M$	KNO_3
$1.4x10^{-4}M$	$MgSO_4 \cdot 7H_2O$
$7.0x10^{-5}M$	$CaSO_4 \cdot 2H_2O$
$8.0x10^{-5}M$	NaCl
$1.4x10^{-4}M$	$NaHCO_3$

The bacteria were determined to be relatively hydrophilic. The contact angle of bacteria grown in mineral medium broth was 34°, see Figure 4 (Appendix B). A hydrophilic polystyrene latex particle (Interfacial Dynamics Co.) with a contact angle of 35.6 ± 5.7° (Wan and Wilson, 1994a) was then used for the colloidal experiments. The colloid was a 0.19 μm carboxylate modified particle with a zeta potential of -52.8 mv, as determined by Wan and Wilson (1994a). Compared to a hydrophobic bacterium, this bacterial strain will be relatively non-sorbing. Of the bacteria that do sorb, the percentage permanently sorbed to the glass surface will be comparatively lower (Wan et al., 1994).

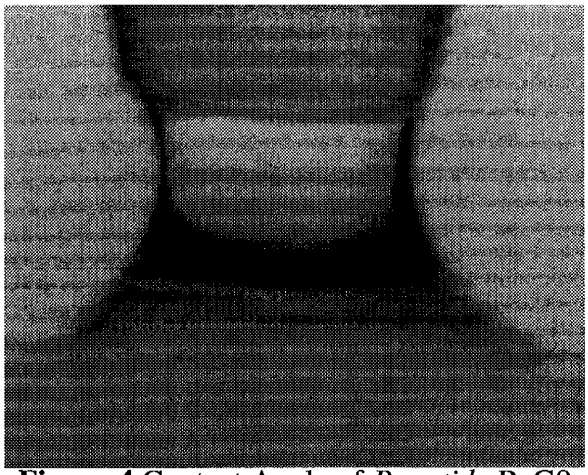

Figure 4 Contact Angle of *P. putida* PpG9
Contact angle was measure to be 34°.

The bacteria were stained by use of CellTracker fluorescent probes (Molecular Probes). CellTracker is a line of stains retained in living cells through several generations. They pass freely through cell membranes, but once inside the cell, they undergo a reaction producing a cell-impermeant reaction product. All the CellTracker dyes contain a chloromethyl reactive group. The reaction is believed to be a glutathione S-transferase-

mediated reaction (Molecular Probes, 1992). This reaction has been shown to occur *in vitro.* We used both Cell Tracker Blue CMHC (micromodels 1, 3) and Cell Tracker Blue CMAC (micromodel 2). All figures shown of fluorescent bacteria stained with Blue CMHC are taken from model 1. Cell Tracker Blue CMHC has a fluorescence excitation wavelength of 354 nm and an emission wavelength of 469 nm. After receiving the stains, a 10 mM solution was made in dimethylsulfoxide. Prior to loading the stains, the cells were centrifuged at 12,100 x g for 10 minutes and the supernatant was removed. The cells were then resuspended in a 25 μM solution of stain in mineral medium. They were then incubated for 45 minutes and recentrifuged. The cells were resuspended in sterile mineral medium and incubated for at least 30 minutes. After this last incubation, the cells were washed again and resuspended in mineral medium for use in the experiment.

B. Optics and Model Set-Up

Three micromodels were constructed according to Wan and Wilson (1994b). The three models were designed to be identical, but due to fabrication techniques there are minute differences. The model pattern, shown in Figure 5, simulates the box experiment that was run at the University of Illinois. The size of the hexagons in the pattern is 1 mm, as is the size of the glass beads used in their box. Because the network pattern is two-dimensional, the micromodel is not an exact replica of the Illinois experiment.

The channel branching at the outflow end of the micromodel reduces preferential flow and short flow paths at the end of the model (Appendix B). Previous model patterns had only a single reservoir at the outflow end. This branching insures that all fluid will be equally mixed and will have to travel a uniform distance to leave the model. This permits sampling at the end of the model to be representative of the entire flow field at the outlet.

The reservoir on the top holds the entrapped NAPL, in this experiment, toluene. The connections between the NAPL reservoir and model pattern are designed so that the NAPL can dissolve into the model but cannot freely flow into the model as a bulk liquid phase. This allows for a dissolved NAPL plume to develop. Tubing is attached at both

ends of the NAPL reservoir. This allows the NAPL be introduced into the reservoir without disrupting the main body of the model, for example after the model is saturated with water and the bacteria are introduced. During the actual emplacement of toluene into the reservoir, some toluene would leak out into the main body of the model. This amount generally occupied 5-10 pores.

The inlet reservoir is also designed with two tubing attachments. This helps in degassing the model during startup. It also allows for a new aqueous solution or suspension to be brought in as a step function. This second aqueous phase can contain colloids, bacteria or a different chemical composition.

Micromodel 1's network has a pore volume of 0.12 ml. By weighing the micromodel before and after filling it with water, the pore volume of the entire model was determined. By measuring the volume of the reservoirs independently, the actual volume in the pattern was determined. The total volume in the reservoirs is 4.59 ml, with the NAPL reservoir having a volume of 1.79 ml.

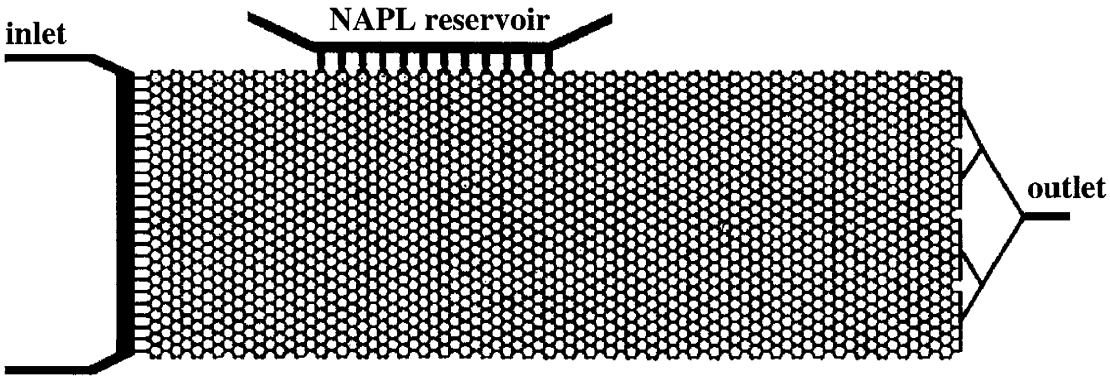

Figure 5 Micromodel pattern used in experiment. The actual pattern measures 16.5 cm from inlet to outlet. The field measures 12.5 cm x 4.5 cm.

We developed a box and filter set-up to hold the micromodel, its plumbing, and various optical filters for visualizing fluorescent bacteria, see Figure 6. Fluorescent bacteria allowed us better visualization and a larger field of view than visible transmitted

light. The box permitted us a full range of motion over the entire micromodel field without being hampered by attached tubing. Finally, we were able to run the experiment vertically, which better simulated Seagren and Rittmann's work.

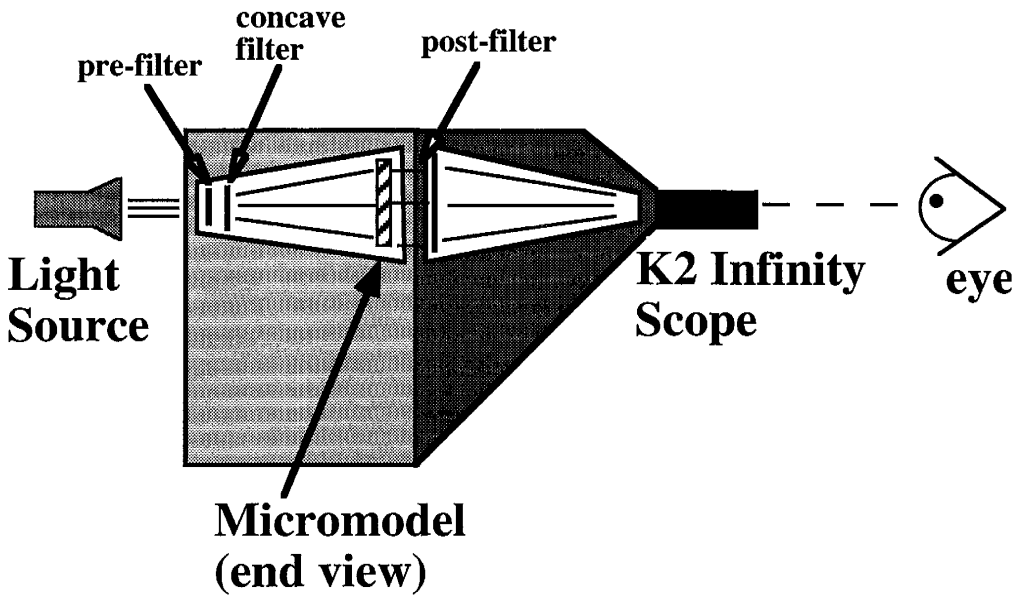

Figure 6 Filter box schematic, side view

The optical filters used for excitation and wavelength cut-off were purchased from Oriel Corp. (Stratford, CT) and Andover Corp. (Salem, NH). The pre-filter is a 2" round Hoya Glass U-330. The post-filter is a 6.5" Schott glass square, GG-420, which allows the viewing apparatus to move around the model without having to move the filter. A concave filter to spread the light after the pre-filter was purchased from Melles-Griot (Irvine, CA). The pre-filter and concave filter were held in holders installed inside the box at the light source opening. The post-filter was held to the opposite end of the box on the outside using c-clamps with Swagelok VCO fittings. The light source was a Phillips flood light. Because the light source was not collimated, there was glare on the model, particularly in the middle.

The micromodel was located inside the box at the end with the post-filter. Tubing ran from the micromodel through holes in the box to syringe pumps (for inlets), flasks

(for outlets), or a sampler, see Figure 7. The tubing was connected to the micromodel using c-clamps with Swagelok VCO fittings.

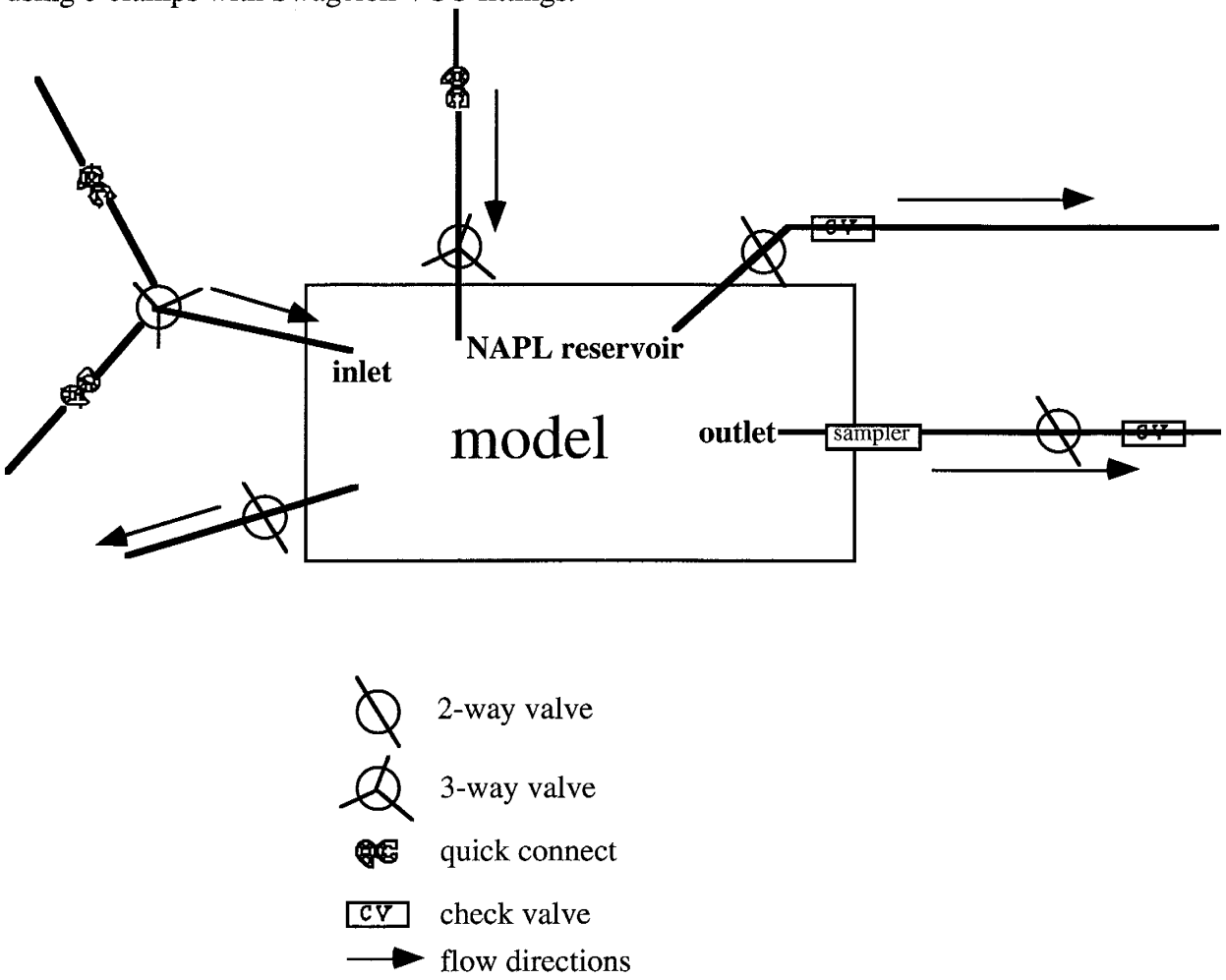

Figure 7 Tubing connection schematic

The K2 Infinity Scope is a long-distance microscope that consists of a series of tubes and lenses. It allows magnification of 2.2x to 52.5x using eyepieces. Photographic images would have a magnification range of 1/2 that. Video magnification ranges from 83.6x to 1995x. Because of the low light conditions, a low-light color CCD camera (Cohu 1310 series camera) was used. Video images were transferred to a Macintosh Quadra 630 using a Radius Video Spigot NuBus card. The contrast on the video images was increased using Adobe Photoshop. This program was also used to remove the glare on the photos (which was replaced with hatched areas), color the solid glass gray and outline the pores.

C. Experiment

Seagren and Rittmann's experimental procedure consisted of two main parts, abiotic dissolution studies and biotic dissolution studies. In both cases, two toluene source strengths (X_{tol}=0.02 and X_{tol}=0.09) and varied velocities were examined. For the biotic dissolution case, the inoculum used was injected into the column and recycled through for 12 hours after which flow was stopped for a minimum of 12 hours to allow time for the bacteria to attach. A start-up phase then followed to encourage bacterial growth throughout the column. After this phase was completed, the toluene-dodecane pool mixtures were added to the column and flow, at the rate of interest, was restarted. Seagren and Rittmann used ^{14}C-labeled toluene so that ^{14}C fractions in all forms, including CO_2 could be measured.

The flow rate used for all our experiments was 0.05ml/hr, which translates to a seepage velocity of 6.1cm/hr. This flow rate of 0.5 pore volumes/hr was selected experimentally as the rate that generated a visible dye plume that extended approximately 3/4 of the way down the model from a dye source in the NAPL reservoir (Appendix C). The flow rate was controlled by a Harvard Apparatus syringe pump, model 44, with a stainless steel 100ml syringe. One-tenth milliliter samples (1 pore volume) were collected from the effluent using a teflon sampling valve (Cole-Parmer). The effluent was dripped into a sample vial containing 1 ml of methylene chloride. The effluent was sampled continuously. A gas chromatograph was then used to determine toluene concentrations. Because of the low sampling volumes, the methylene chloride was used to capture all the toluene from the aqueous phase and limit volatilization. Despite the use of methylene chloride, limited volatilization did occur. This was not quantified but noted by seeing less sample in the vial than in the typical vials.

For each of the three micromodels, the toluene dissolution experiment was run under three different conditions. The first condition was a control without colloids or bacteria. The model was saturated with mineral medium and then neat toluene (Fisher

Scientific) was introduced into the NAPL reservoir. The samples collected at the outlet represented the mass of toluene in the effluent during the experiment. This series of experiments was run for 60 hours. The second condition acted as an additional control for the experiment. A suspension of hydrophilic latex particles with contact angle similar to the bacteria were introduced into the micromodel. The suspension was 0.42% solids or 1.13×10^{12} particles/ml. The suspension was run through the mineral medium saturated micromodel at the indicated flow rate for 12 hours, and then the flow was stopped for 12 hours. This allowed time for attachment to the micromodel. Although very little attachment by the abiotic colloids was expected, the step was included to match procedures with the bacterial condition. The toluene was then introduced into the top reservoir and flow was restarted. The effluent was collected every other hour. Effluent pH was measured as 7.0, as measured in random samples using pH paper. So that concentrations of abiotic colloids would be great enough to be visible, any colloidal suspension remaining in the inlet lines was flushed out 48 hours after the toluene was introduced into the reservoir. The experiment was continued with particle free water for an addition 24 hours. This set of experiments was run for 72 hours. The position of the colloids was recorded every 24 hours.

Any differences in toluene mass collected between controls were presumably due to the presence of colloidal material, primarily due to toluene partitioning onto the abiotic colloids. The position of the abiotic colloids relative to the contaminant plume was observed before and after introduction of the toluene. This indicated any changes in colloid attachment and distribution purely due to mechanical or chemical forces.

The third condition was the actual biotic experiment. This experiment was set-up to closely imitate Seagren and Rittmann's experimental procedure, excluding the start-up phase and not using ^{14}C-labeled toluene. This condition was run identically to the abiotic colloids method, with two procedural exceptions. One change in procedure was that all equipment; clamps, tubing, syringes, micromodel and mineral medium, were

sterilized by autoclave prior to use. The o-rings on the VCO fittings were sterilized by UV exposure for 12 hours. The second change was that any bacteria in the inlet reservoir were flushed out at t=0 so that the incoming fluid contained only the mineral medium. The incoming bacterial concentration was about 10^6 CFU/ml as measured by plate counts. A sample of the incoming fluid was collected for plate counts using the spread plate method. The position of the bacteria in the micromodel was noted every 24 hours.

For photographic purposes, this last condition was run a second time in micromodel 1 using unstained bacteria. No effluent samples were collected. A Zeiss stereoscope was used for magnification.

D. Effluent Sample Measurements

The effluent was collected in methylene chloride. The effluent flowed through a needle whose tip was in the methylene chloride. One milliliter of methylene chloride was in a crimp top GC vial (Alltech) with the top in place. The effluent was sampled continuously. Vials were exchanged every two hours, except at night. Because an auto-sampler could not be used, night time samples were left on for longer periods of time. The two hour samples weren't vented, but the overnight samples were.

After collection, the samples were immediately analyzed on a Hewlett-Packard GC model 5890A with FID detector. Operating conditions are shown in table 3. Data was analyzed as peak areas and compared to standards of 100 mg/l purchased from Alltech. Sample concentrations ranged from none detected to saturation (515 mg/l). Detector response was assumed to be linear. Standards were run straight from the bottle and as 0.1 ml in one ml methylene chloride. The 0.1 ml standards showed a 79% recovery of toluene from the methylene chloride. This was taken into account when experimental sample concentrations were calculated. On the GC, blanks of water and methylene chloride were run. Standards and blanks were run every 10 or fewer samples.

Table 3 Operating conditions for gas chromatography equipment for analysis of toluene in methylene chloride.

Carrier Gas:	Helium: 5.56 - 5.88 ml/min
Make-up Gas:	Nitrogen: 24.12 - 26.44 ml/min
Hydrogen:	57.12 - 59.44 ml/min
Air:	385 - 390 ml/min
Septum Purge:	1.21 ml/min
Split Vent:	34 - 35 ml/min
Initial Oven Temperature:	50° C
Injector Temperature:	200 ° C
Detector Temperature:	250° C
Split Ratio:	7:1
Purge A:	On
Purge B:	On
Threshold:	0
Attenuation:	2
Zero:	0
Peak Width:	0.04
Area Rej.:	0
Chart Speed:	1.0

Temperature Program: Initial temperature 50° C, held for 3.0 minutes, ramped 10° C/minute from 3-7 minutes, then ramped 20° C/minute from 7-9 minutes to a maximum oven temperature of 125° C. Total run time for each sample was approximately 13 minutes (including the time require for the oven temperature to be reset to initial temperature).

The effluent concentration data were changed into mass of toluene collected and totaled over the 72 hours of the experiment to give cumulative mass of toluene collected. This data transformation was used because the concentration data were erratic. Because only 0.1 ml was sampled over the two hours, each individual sample may have contained more or less than 0.1 ml, depending on whether one or two drops were collected. This would be partially compensated for by taking the cumulative value.

VIII. Results and Discussion

The total mass of toluene collected in the effluent, relative to controls, was reduced when bacteria were present, see Table 4. Although the amounts were not statistically different due to the small sample size and large standard deviation, they do indicate a trend. The large deviation between models points to the difficulties in getting quantitative data from micromodels. These difficulties include: detailed differences between micromodels, low model volume and subsequent low sample volume and problems with accessing the fluid in the model. These data should be looked upon not as absolute numbers but as indicators. Seagren (1994) found that even when no enhanced dissolution occurred, the mass of toluene collected was lower because some of the ^{14}C came out as degradation products. In this study, it could not be determined whether the lower mass collected in the bacterial experiments was due to biodegradation, sorption onto the bacteria or a separate mechanism, such as clogged pores preventing diffusion. Toluene sorption onto the bacteria may have occurred in Seagren's work; this would mask any enhanced dissolution in the high concentration experiments. On average, the presence of abiotic colloids showed little influence on the toluene mass collected.

Table 4 Cumulative mass collected for the three experimental conditions.

	Mass of toluene collected (mg)			
experimental condition	model 1	model 2	model 3	average
blank	1.92	1.10	0.86	1.30±0.56
abiotic colloids	1.09	0.09	2.55	1.24±1.24
bacteria	0.01	0.21	1.10	0.44±0.58

The mass recovered is the cumulative amount recovered over the course of the experiment (72 hours). The averages were determined from the values of the three different micromodels.

The abiotic colloids were uniformly distributed in the presence of toluene. Figure 8 shows that 48 hours after the toluene was introduced, the colloidal concentration beneath the toluene reservoir was uniform. The incoming fluid for those 48 hours was a colloidal suspension. The photograph taken immediately after the toluene was introduced

shows a slight amount of colloidal suspension towards the bottom of the model. This was taken immediately after the 12 hour rest period, when no flow was passing through the model. I do not know the cause of this behavior, but the reason for the lack of observable colloids may be due to settling of the colloids during those 12 hours. The uniformity at 48 hours, when colloids can be seen, indicates that if the bacteria colonize in a specific place (e.g., the boundary-layer region) this colonization would be due to the biological effect of toluene on the bacteria and not due to surface chemistry.

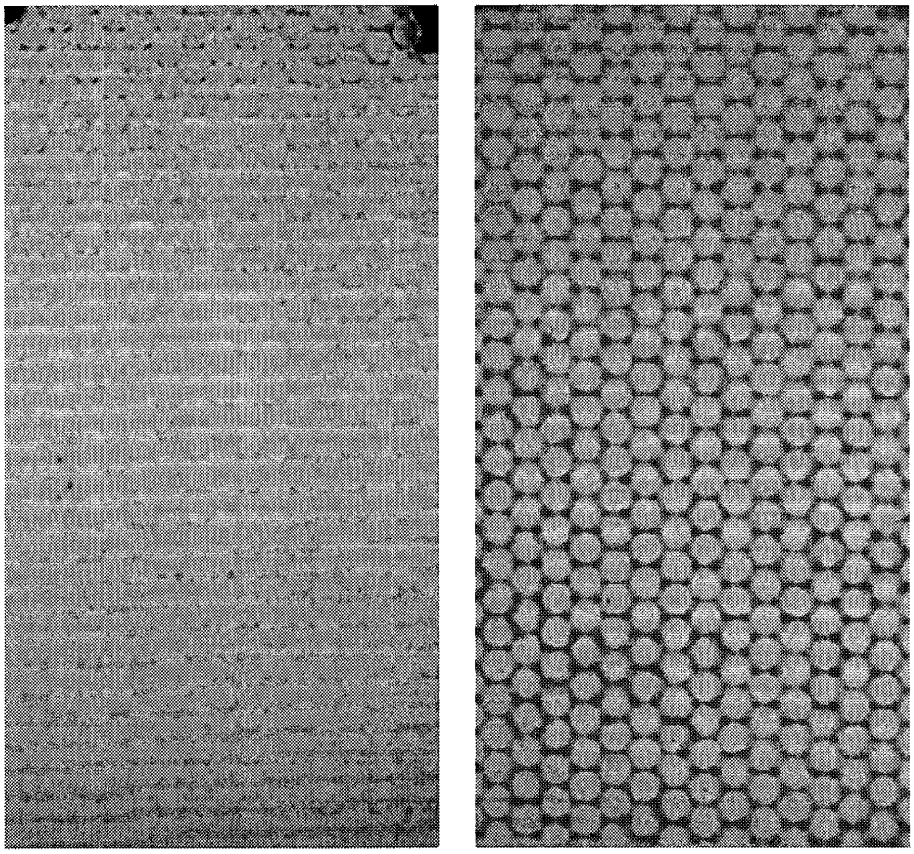

t=0h **t=48h**

Figure 8 Colloidal distribution beneath the toluene reservoir. Darker gray indicates higher concentrations of colloids. T=0 is immediately after toluene was introduced into the reservoir. The lack of colloids in at t=0 may be due to settling.

To track the colonization of the bacteria, the three different areas of the model highlighted in Figure 9, were examined closely. These areas all lay within the boundary-layer region and were expected to show biological activity, especially growth. A single pore was selected as representative of the areas. Many pores in the areas, besides the

shown pore, were looked at also. The representative pore was similar to all the nearby pores (Appendix D).

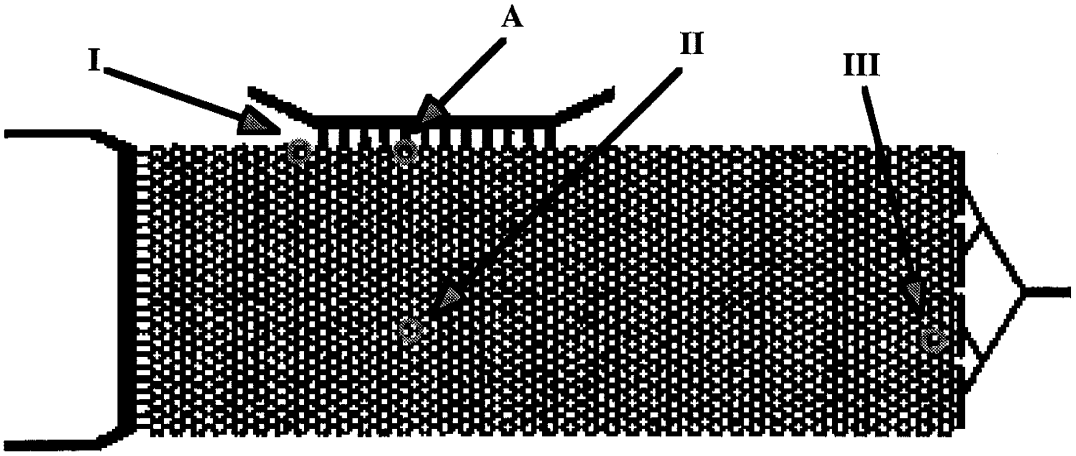

Figure 9 Areas tracked during bacterial colonization experiment. Areas I, II, and III were closely followed throughout the experiment. They are in the boundary-layer region.

Figure 10 shows video images of how the growth progressed in the three areas during the course of the experiment. The stills were taken 24 hours apart at 0, 24, 48, and 72 hours, with zero hours being immediately after the introduction of toluene. Area I shows an increase in bacteria. This increase is not steady. The increase occurs adjacent to a toluene blob. Area II shows little or no activity. Area III also shows very little biological activity throughout the experiment. This indicates that our hypothesis of preferential colonization in the boundary-layer region is rejected.

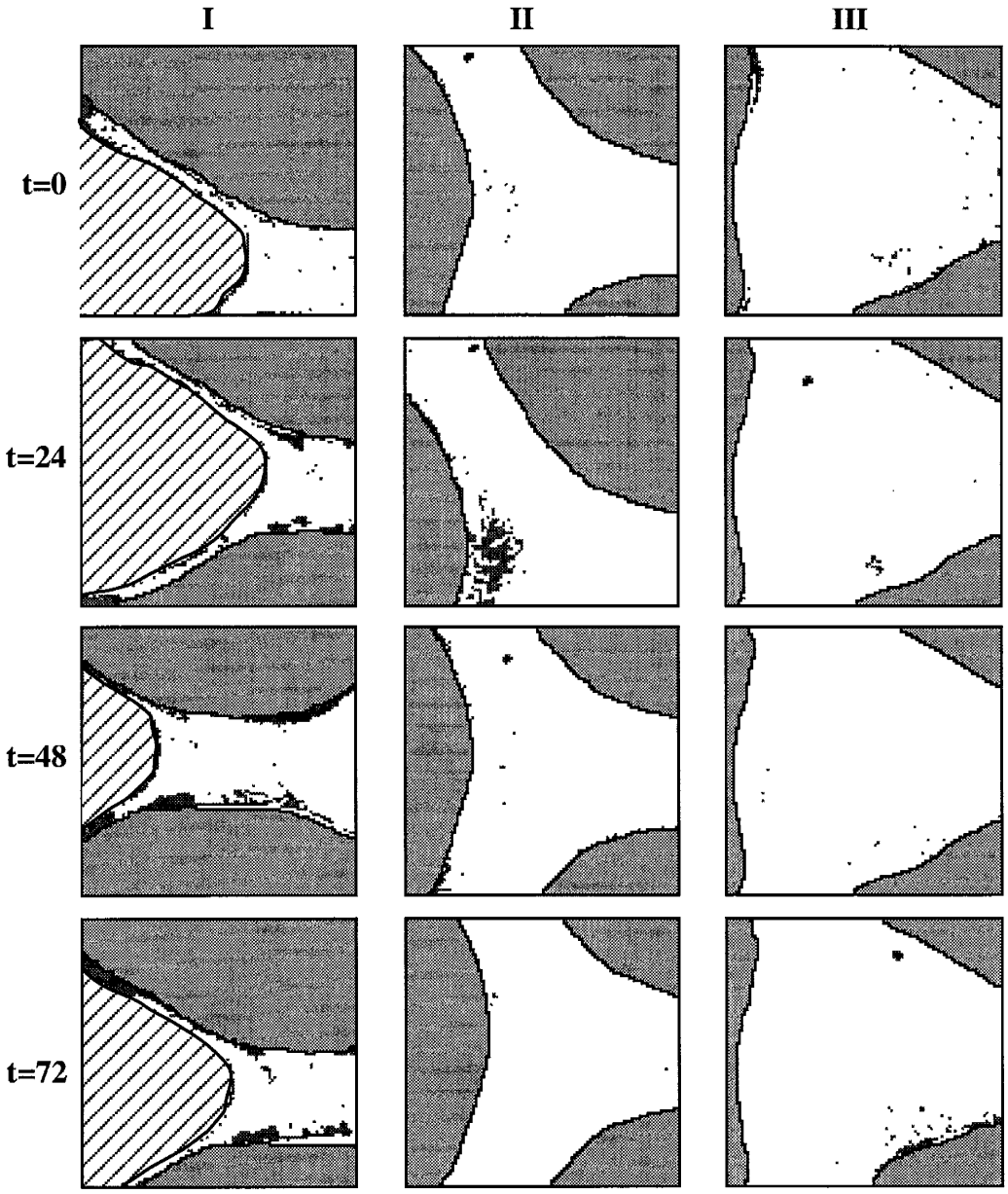

Figure 10 Position of bacteria in areas tracked over time. The bacteria appear as dark gray specks. Some of the pores show gray on the left due to video tape noise. Images, as shown, are 55x. Solid areas are colored light gray. All pictures in a column are of the same pore. The hatched area in Area I is toluene, as a seperate phase. T=0 is immediately after the toluene was introduced.

Seagren's experimental work suggested that most of the biological activity was taking place in the top centimeter of the column (Seagren, 1994). He also showed that when the toluene concentration was raised, the biomass decreased. In the column with the higher toluene concentrations, the biomass was more spread out and the amount of

biomass was much lower directly below the toluene pool. We used a pure toluene pool and had expected the trend to continue that at higher concentrations the bacteria were further from the toluene source and fewer cells were directly below the source. However, because we didn't see any enhanced activity in the boundary-layer region, we decided to look near the pool (area A, fig. 9). Figure 11 shows colonization at area A, with the population increasing through 48 hours after the toluene was introduced. This biological activity was not anticipated as the concentrations at that area should be inhibitory or even toxic. The glare in these stills has been removed and replaced by a hatched area. No visual data is available for these hatched areas because of the glare. The presence of the glare may also account for the lack of bacteria visible at 24 hours. A closer look directly above area A shows the bacteria moving up into the reservoir, see Figure 12. This movement occurred between 24 and 48 hours after the introduction of toluene. The toluene in this reservoir should be toxic and not support any bacteria. The bacteria were noted at the surface of the toluene and not inside the seperate phase. Because the toluene was put into the reservoir after the model had been saturated with mineral medium, there is a thin water film surrounding the toluene. It is in this thin film that the bacteria are colonizing.

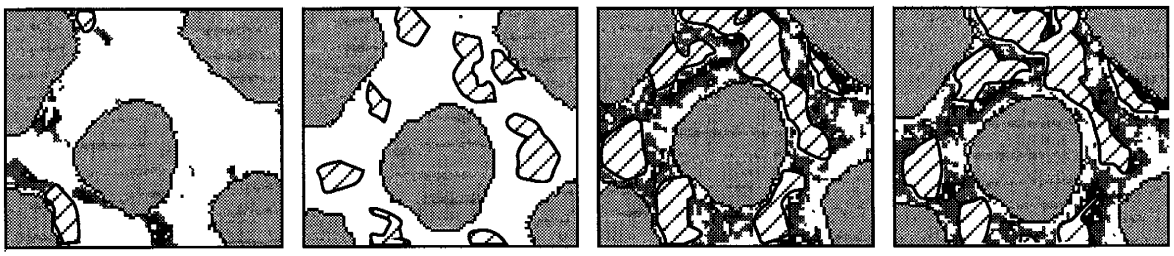

Figure 11 Bacteria colonizing in area A. The bacteria appear as dark gray areas. The large, light gray areas are solid. The glare has been removed and is indicated by the hatch pattern. These images, as shown are 15x.

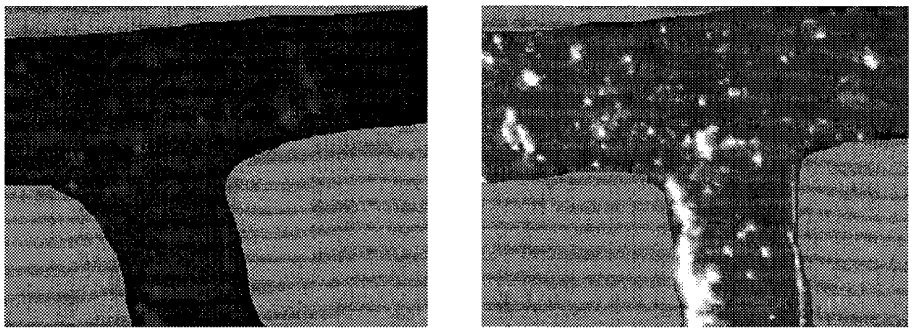

t=0 t=48

Figure 12 Bacteria in the reservoir. This part of the reservoir is directly above area A and is shown at 15x. These bacteria appear as white specks. There is glare to the left of the descending pore at t=48.

Although there is no experimental proof, three potential explanations for this behavior exist; a different bacterial type was being observed at area A; the toluene concentration encountered by the bacteria was much lower than predicted; or the bacteria could be toluene-tolerant. The interpretation must also help explain the lower toluene mass collected.

The bacteria could be of a different type due to contamination or mutation; or they might even be dead. All equipment, including tubing and the micromodel, was sterilized prior to use. In order for a contaminant bacterial strain to exist in area A and be seen, it would have to have been stained or be naturally fluorescent. More importantly, this strain would have to be toluene-tolerant. Because of these requirements and the care taken to prevent contamination, we feel that this is not a probable explanation. We also feel the mutation explanation is inadequate. It is probable that this strain, PpG9, could produce a toluene-tolerant or otherwise advantaged mutant. Although advantageous mutations occur more frequently when the cells are environmentally challenged (Hall, 1990), the mutation rate would be inadequate to produce enough mutants to be seen during the course of the experiment.

Toluene affects the membranes of bacteria and is used to lyse microbial cells. Because of this we would expect cells in area A to be dead. The stain we used was an intracellular stain. If a cell died and its membrane was disrupted, the stain would leave

the cell. The cell would no longer be visible (Molecular Probes, personal communication, Sept. 1994), so it is unlikely that the increase in bacteria we see in area A and the reservoir is due to visualization of an accumulation of dead cells.

A lower toluene concentration encountered by the bacteria could be a result of limited diffusion due to a barrier between the toluene source and the bacteria. There are two possible types, both of which would lead to a lower toluene mass being collected in the effluent. The first type of barrier would be a partial clogging of the pores near the reservoir. This clogging could be accomplished by sorption of dead cells or cellular components onto the glass. We did not see any biomass large enough to cause such a blockage.

The second barrier could be a protective coating over live cells sorbed at or near the NAPL-water interface. This protective coating could be from extracellular polysaccharide production. Extracellular polysaccharides are produced in higher quantities by cells attached at a solid-liquid interface than by those unattached (Vandevivere and Kirchman, 1993). The attachment period prior to the introduction of the toluene may have allowed some cells to develop a polysaccharide coating. The introduction of toluene may also have stimulated polysaccharide production and coating. An extracellular polysaccharide protective coating would allow bacteria to grow at the toluene-water interface by providing a barrier to the high toluene concentrations. These bacteria would encounter low toluene concentrations at their cell walls which they could utilize, leading to a lower toluene mass being collected in the effluent.

Certain polysaccharides can complex with proteins to form microbial biosurfactants (Thangamani and Shreve, 1994). These surfactants can be released into the surrounding environment. By looking at the micromodel under a microscope (Zeiss Axiophot) after the experiment was over (all tubing was disconnected), microscopic droplets were discovered, see Figure 13. These droplets were in areas that had contained visible toluene blobs which had leaked out of the reservoir during emplacement. These

could have been from an emulsion caused by biosurfactants. More support of the polysaccharide theory is the wetting behavior of the toluene. Toluene is non-wetting in the micromodels. In areas where biomass was observed, the toluene's wetting behavior was altered. Also, in microbial adhesions to hydrocarbon assays, cells grown on toluene showed greater adhesion to the hydrocarbon than those grown on tryptic soy broth (Appendix B). It has been shown that the presence of a biosurfactant can affect assay results by increasing adherance to the hydrocarbon (Zhang and Miller, 1994). Although no biosurfactants could be identified, the wettability changes, increased hydrocarbon adherance and droplets indicate that they may be present. These surfactants could be polysaccharide-protein complexes, suggesting the presence of a polysaccharide protective coating.

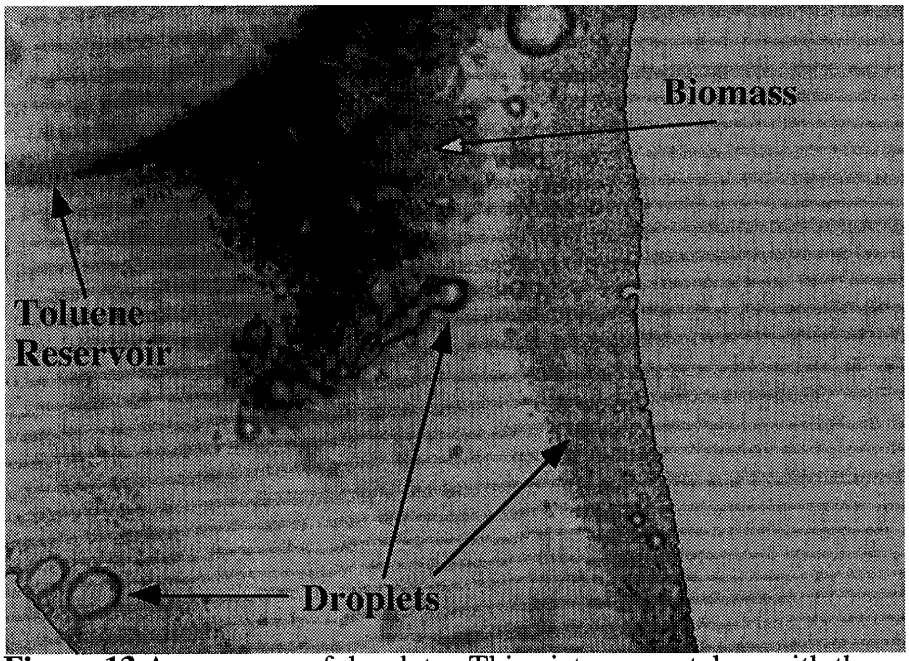

Figure 13 Appearance of droplets. This picture was taken with the model under a Zeiss axiophot microscope at a magnification of 320x. The droplets appear to be sorbed to the glass surface. This is in area A. This photomicrograph was taken at t=72+ h, after the experiment was over.

It is also possible that the bacteria are toluene-tolerant. Toluene-tolerant *Pseudomonas* strains have been shown to thrive at concentrations higher than 50% v/v (Inoue and Horikoshi, 1989; Aono et al., 1992; Nakajima et al., 1992). This strain is not

that tolerant (Seagren, 1994). Toluene-tolerant mutants have been found in *Pseudomonas putida* strains (Shima et al., 1991). The mutation rate for this strains varies from 10^{-8} to 10^{-9}, which is too low to be seen during the course of this experiment. It has been shown that *P. putida* can adapt (Weber et al., 1994). Weber et al studied different *P. putida* strains that were able to adapt to high concentrations of toluene by changing their membrane composition. The membrane change was an increase in *trans* fatty acids which decrease the fluidity of the membrane. These bacteria were able to tolerate toluene concentrations of up to 400 mg/l. The solubility of toluene in water is 515 mg/l (Verschueren, 1983). This membrane change occurred when the bacteria were grown in the presence of toluene. This may explain the toluene-tolerant behavior of *P. putida* PpG9 I observed. The bacteria had been grown in the presence of toluene for several generations prior to inoculation into the model. It has been shown that *P. putida* PpG9 shows a change at the cell surface when grown on toluene (Appendix B). Cells grown on toluene had a different contact angle than cells grown in tryptic soy broth. These toluene-tolerant bacteria could then situate directly below the toluene pool and degrade some of the dissolved toluene. This also would lead to lower mass being collected in the effluent.

Both the toluene degradation by toluene-tolerant cells and/or polysaccharide coated cells would cause the boundary-layer region to move from the position previously determined. This region was defined using a dye solution in the model's NAPL reservoir prior to the start of the experiments. I could not determine whether the boundary-layer region moved during this experiment.

IX. Conclusions

The surface chemistry of the bacteria, as determined by contact angle, was not responsible for the position of the bacteria in the contaminant plume. Colloids with a similar contact angle were uniformly distributed throughout the model in the presence of the toluene.

The bacterial colonization close to the contaminant source and subsequent movement into the reservoir was not anticipated. The hypothesis that the bacteria would colonize a region where the toluene concentrations were low was not supported.

The presence of bacteria in the micromodel caused an apparently lower mass of toluene to be collected. The mechanism which caused the toluene decrease could not be determined. Potential reasons for this effect are: biodegradation of the toluene, sorption onto the bacteria or a barrier limiting diffusion out of the toluene reservoir. These phenomena may have happened individually or together.

Two hypothetical explanations for the observation of bacteria at the NAPL-water interface are the existence of a barrier to limit diffusion and an adaptation by the bacteria to become more toluene-tolerant. This barrier could be due to an extracellular polysaccharide protective coating around the cells. The toluene-tolerance would be as a result in adaptations by the outer cellular membrane. It is possible that both the barrier and adaptation occurred and worked in concert to increase growth at the NAPL-water interface.

X. Future Work

Work evolving from this thesis can be classified into four categories. The first is reworking two of the early phase experiments; the contact angle work and the reservoir end work. Secondly, there could be refinement of the visualization technique. The third would be extensions of this work into other conditions. The final category would be to check the speculations that arose from my results.

The early phase of work that could be refined involved testing the micromodel ends and the bacterium's contact angle. The micromodel end test showed that branching does indeed lead to better sampling of the effluent (Appendix B). This work could be refined by using two micromodels with the same pattern, excepting the end reservoir. The effect of growth media upon bacteria contact angles (Appendix B) could be retested using a new, possibly more accurate method for measuring contact angles. A new method, the captive drop centrifugation method, is currently being developed (Flinsch and Wilson, 1994). This method would have to be further developed to allow for water/air systems to be investigated.

Although I developed the technique used to visualize the bacteria in the micromodel, I feel that this technique still has room for much improvement. Of particular importance would be the finding of a better light source. The light source being used provides me with light that is in the color range I need, but a brighter, more intense light would help visualizing the bacteria. Because of light limitations, I had a hard time seeing the bacteria in the model, especially due to glare. I used a 1500K floodlight. Phillips has come out with a flood light with a higher temperature rating; this may yield some improvements. A collimator on the light would also help.

The Infinity Scope stand could also be improved. This stand was cobbled together using parts from different companies. Because of this there are many joints that cause the scope to wiggle, introducing jitters into the image. I also feel that although the box is

good, a better set-up would be to have the filters in stands on a long vibration free surface that is made for optical work. This could be a vibration dampening breadboard on top of current tables or countertops, or an optical table on its own.

In a similar vein of improving technique would be improving toluene sampling and analysis. Control of volatilization and sample size would greatly improve effluent sampling. The analysis needs better quality control in the GC and associated measurements.

The third category is most interesting. This work could be expanded using different circumstances very easily. Other contaminants could be used, such as benzene and xylene, alone or in mixtures. These are similar to toluene and can be degraded by the same bacteria. This would give a more complete picture of bacterial reactions to gasoline spills. Besides LNAPLs, DNAPLs could also be used. Other things that could be looked into would be changes in the bacteria's living conditions, such as pH, Eh, and oxygen availability. Other bacteria could also be looked into as well as mixed populations.

Category four would be checking on the possibilities of barrier limited diffusion or acquired toluene-tolerance. To check if this strain will acquire toluene-tolerance, work can be done in flasks and other standard culture containers by using a method similar to that presented in Weber et al (1994). They grew bacteria in the presence of low levels of toluene and then added toluene. These resultant higher concentrations would kill the bacteria if added to non-tolerant cells. If the bacteria were able to acquire toluene-tolerance, growth would occur in the presence of high toluene concentrations when the bacteria had been previously exposed to low concentrations. Checking for barrier limited diffusion will be more difficult. A check for increased polysaccharide production due to attachment and the presence of toluene could be made by using methodology based upon Vandevivere and Kirchman (1993). They used colorimetric methods to detect extracellular polysaccharides and cell-bound exopolymers synthesized by attached and unattached bacteria in continuous-flow columns. The influence of toluene on exopolymer

synthesis could be investigated by using varying concentrations of toluene in the feed solution. The effect of residual toluene in the column could also be investigated.

XI. References

Alvarez, P.J.J., P.J. Anid, R.M. Vogel. 1991. Kinetics of Aerobic Biodegradation of Benzene and Toluene in Sandy Aquifer Material. Biodegradation. 2:43-51.

Aono, R., M. Ito, A. Inoue, and K. Horikoshi. 1992. Isolation of Novel Toluene-Tolerant Strain of *Pseudomonas aeruginosa*. Biosci. Biotech. Biochem. 56:145-146.

Borden. R.C., P.B. Bedient. 1986. Transport of Dissolved Hydrocarbons Influenced by Oxygen-Limited Biodegradation 1. Theoretical Development. Water Resources Research. 22:1973-1982.

Conrad, S.H., J.L. Wilson, W.R. Mason, and W.J. Peplinski. 1992. Visualization of Residual Organic Liquid Trapped in Aquifers. Water Resource Research. 28:467-478.

Ellwood, D.C., J. Melling, P. Rutter, Ed. 1979. *Adhesion of Microorganisms to Surfaces*. Academic Press, NY.

Flinsch, M., J. Wilson. 1994. Estimation of Bacterial Hydrophobicity from Contact Angle Measurements: an Improved Method. AGU Fall Meeting. H31C-6.

Hall, B.G. 1990. Spontaneous Point Mutations That Occur More Often When Advantageous Than When Neutral. Genetics. 126:5-16.

Harvey, R.W., M.A. Widdowson. 1992. Microbial Distributions, Activities, and Movement in the Terrestrial subsurface: Experimental and Theoretical Studies. In R.J. Wagner, P. Baveye, B.A. Stewart (Eds), *Interacting Processes in Soil Science*. Lewis Publishers. pp 185-225.

Inoue, A., K. Horikoshi. 1989. A *Pseudomonas* Thrives in High Concentrations of Toluene. Nature. 338:264-266.

MacQuarrie, K.T.B., E.A. Sudicky, E.O. Frind. 1990. Simulation of Biodegradable Organic Contaminants in Groundwater 1. Numerical Formulation in Principal Directions. Water Resources Research. 26:207-222.

Miller, C.T., M.M. Poirier-McNeill, and A.S. Mayer. 1990. Dissolution of Trapped Nonaqueous Phase Liquids: Mass Transfer Characteristics. Water Resource Research. 26:2783-2796.

Molecular Probes. Dec. 30, 1992. CellTracker™ New Fluorescent Probes for Long-Term Tracking of Living Cells. MP Bulletin 2925.

Molz, F.J., M.A. Widdowson, L.D. Benefield. 1986. Simulation of Microbial Growth Dynamics Coupled to Nutrient and Oxygen Transport in Porous Media. Water Resources Research. 22:1207-1216.

Nakajima, H., H. Kobayashi, R. Aono, and K. Horikoshi. 1992. Effective Isolation and Identification of Toluene-tolerant *Pseudomonas* Strains. Biosci. Biotech. Biochem. 56:1872-1873

Powers, S.E., C.O. Loureiro, L.M. Abriola, and W.J. Weber, Jr. 1991. Theoretical Study of the Significance of Nonequilibrium Dissolution of Nonaqueous Phase Liquids in Subsurface Systems. Water Resources Research. 27: 463-477.

Seagren, E.A. 1994. Biodegradation of Poorly Soluble Organic Contaminant. Unpublished thesis.

Seagren, E.A., B.E. Rittmann, A.J. Valocchi. 1993. Quantitative Evaluation of Flushing and Biodegradation for Enhancing in situ Dissolution of Nonaqueous-phase Liquids. J. Cont. Hyd. 12:103-132.

Seagren, E.A., B.E. Rittmann, and A.J. Valocchi. 1994. Quantitative evaluation of the enhancement of NAPL-pool dissolution by flushing and biodegradation. Environ. Sci. Technol. 28:833-839.

Shima, H., T. Kudo, and K. Horikoshi. 1991. Isolation of Toluene-resistant Mutants from *Pseudomonas putida* PpG1 (ATCC 17453). Agric. Biol. Chem. 55:1197-1199.

Thangamani, S. and G.S. Shreve. 1994. Effect of Anionic Biosurfactant on Hexadecane Partitioning in Multiphase Systems. Environ. Sci. Technol. 28:1993-2000.

Vandevivere, P. and D.L. Kirchman. 1993. Attachment Stimulates Exopolysaccharide Synthesis by a Bacterium. Applied and Env. Micro. 59:3280-3286.

Verschueren, K. 1983. *Handbook of Environmental Data on Organic Chemicals, 2nd Ed.* Nostrand Reinhold Co. New York.

Wan, J., and J.L. Wilson. 1994a. Colloid Transport in Unsaturated Porous Media. Water Resources Research. 30:857-864.

Wan, J. and J.L. Wilson. 1994b. Visualization of the Role of the Gas-Water Interface on the Fate and Transport of Colloids in Porous Media. Water Resources Research. 30:11-23.

Wan, J., J.L. Wilson, and T.L. Kieft. 1994. Influence of the Gas-Water Interface on Transport of Microorganisms through Unsaturated Porous Media. Applied and Env. Micro. 60:509-516.

Weber, F.J., S. Isken and J.A. de Bont. 1994 *Cis/Trans* Isomerization of Fatty Acids as a Defense Mechanism of *Pseudomonas putida* Strains to Toxic Concentrations of Toluene. Microbiology. 140:2013-2017.

Yanagita, T. 1990. *Natural Microbial Communities.* Japan Scientific Press, Tokyo.

Zhang, Y. and R.M. Miller. 1994. Effect of a *Pseudomonas* Rhamnolipid Biosurfactant on Cell Hydrophobicity and Biodegradation of Octadecane. Applied and Env. Micro. 60:2101-2106.

XII. Appendices

A. Appendix A

1. Illinois Experiment

Introduction

1. Remediation of subsurface contamination by nonaqueous phase liquids (NAPLs) is currently one of the major challenges in groundwater remediation (Bedient, 1991). Migration of spilled NAPL through pore spaces as a separate phase traps significant volumes of NAPL in the porous medium in the form of discrete ganglia (blobs) or continuous pools (e.g., Mercer and Cohen, 1990). This entrapped NAPL represents a long-term groundwater pollution source whose remediation is often dependent on interphase transfer, such as NAPL dissolution, and its enhancement. Two remediation techniques are flushing (i.e., pump-and-treat) and *in situ* biodegradation. Whether in a separate liquid phase or sorbed to aquifer solids, these poorly soluble compounds cannot easily be flushed from the subsurface by water extraction. On the other hand, bacterial activity can destroy contaminants and accelerate dissolution, if the bacteria are located close enough to the interface between the water and the adsorbed or liquid-phase contaminant.

2. Using a combination of experimental and modeling approaches, this work quantifies NAPL pool dissolution and its enhancement by flushing and *in situ* bioremediation. The fundamental hypothesis of this research is that *in situ* biodegradation of the dissolved NAPL components can serve as a significant sink term for solute and cause an increase in the concentration gradient in the aqueous phase, resulting in an increase in NAPL dissolution above that produced by flushing alone. Bacteria able to locate near the interface will give the greatest effect.

3. Experiments and modeling were performed with toluene, a very commonly encountered hydrocarbon that is characterized by being relatively soluble and inhibitory to bacteria when present at high enough concentrations. Our preliminary experiments with toluene and *Pseudomonas putida* PpG9 demonstrated that toluene was rapidly

biodegraded, but only when its aqueous-phase concentration was substantially less than the solubility of pure liquid toluene (i.e., 515 mg/l at 20°C (Verschueren, 1983)).

Modeling

4. Biological reaction is not the only mechanism that reduces the liquid-phase concentration of a NAPL: Advection and dispersion also serve as solute "sinks," In fact, flushing, which is a key component of pump-and-treat technology, relies on advection to remove dissolved contaminant and accelerate NAPL removal. We used a modeling analysis to develop quantitative tools for assessing when biological activity significantly increases NAPL dissolution over that which can occur through flushing. The details of the model development and application are given in Seagren et al. (1993; 1994).

5. The interactions of NAPL dissolution, biodegradation by attached bacteria, and solute transport are evaluated for two simple domains: immobilized blobs in a saturated, homogeneous, isotropic medium with one-dimensional flow, and a NAPL pool adjacent to a saturated, isotropic medium having two dimensions.

Blob Dissolution in a One-Dimensional Domain

6. The steady-state mass-balance equation for dissolution of a biodegradable solute from uniform blobs in one-dimensional flow is

$$0 = \frac{\partial C}{\partial t} = D_x \frac{\partial^2 C}{\partial x^2} - \frac{q_x}{nS_w}\frac{\partial C}{\partial x} + R_B + R_D \quad (1)$$

in which C = NAPL-solute concentration [ML^{-3}]; t= time [T]; D_X, = longitudinal dispersion coefficient [L^2T^{-1}]; x = distance in the direction of flow [L]; q_X, = specific discharge [LT^{-1}]; n = porosity; S_W = water saturation; R_B = biodegradation sink term [$ML^{-3}T^{-1}$]; and R_D = dissolution source term [$ML^{-3}T^{-1}$]. The dissolution rate was described by a first-order interphase mass-transfer relationship:

$$R_D = k_1(C_s - C) \quad (2)$$

in which C_S = the solubility concentration of the pure NAPL [ML^{-3}] and k_1 = a lumped interfacial mass-transfer coefficient [T^{-1}] that depends on hydrodynamics and the NAPL's specific surface area. The biodegradation rate is modeled as a pseudo-first order:

$$R_B = -k_{B1}C \quad (3)$$

in which k_{B1} = a lumped first-order rate coefficient [$ML^{-3}T^{-1}$] that includes the amount of attached biomass (assumed constant in the domain) and the solute's intrinsic biodegradation kinetics.

7. Equations (1)-(3) were combined and converted to a dimensionless format that includes three dimensionless group parameters:

$$0 = \frac{1}{Pe}\frac{d^2C^*}{dx^{*2}} - \frac{dC^*}{dx^*} - (Da_1 + Da_2)C^* + Da_1 \quad (4)$$

in which C^* = a dimensionless concentration C/Cs, x^* = a dimensionless distance = x/L, L = the length of the domain [L], and three dimensionless group parameters are defined in Table 1. Table 1 also defines a fourth group, Da_3, which equals Da_2/Da_1. Boundary conditions are of the third type for the inlet

$$\left(-\frac{1}{Pe}\frac{dC^*}{dx^*} + C^*\right)_{x^*=0} = 0 \quad (5)$$

and for a semi-infinite domain for the outlet,

$$\frac{dC^*(\infty)}{dx^*} = 0 \quad (6)$$

The analytical solutions for $C^*(x^*)$ and a normalized dissolution rate (rd^*) are given as functions of Pe, Da_1, and Da_2 by Seagren et al. (1993).

Table 1 Definitions of Dimensionless Group parameters

$$Pe = \frac{\text{advection rate}}{\text{dispersion rate}} = \frac{V_x L}{D_x} \quad (7)$$

$$Da_1 = \frac{\text{mass} - \text{transfer rate}}{\text{advection rate}} = \frac{k_1 L}{V_x} \quad (8)$$

$$Da_2 = \frac{\text{biodegradation rate}}{\text{advection rate}} = \frac{k_{B1} L}{V_x} \quad (9)$$

$$Da_3 = \frac{\text{biodegradation rate}}{\text{mass} - \text{transfer rate}} = \frac{k_{B1}}{k_1} \quad (10)$$

Note: V_X = average pore water velocity = q_X /(n S_W)

8. Figures 1 and 2 summarize the most important findings:

•Maximum dissolution rates (i.e., rd* = 1 or C* = 0) can be achieved by increasing flushing so that Da1 <0.01 or by increasing biodegradation so that Da3 > 100.

•Increasing biodegradation effects a significant increase in the dissolution rate (and decrease in C*) only when Da3 increases through the range 0.01 to 100.

•If flushing already is decreasing C* (i.e., Da1 < 0.01), increases to biodegradation have little added benefit for increasing the dissolution rate.

9. These findings define the ranges of Da_1, Da_2, and Da_3 in which flushing and/or enhanced biodegradation can accelerate NAPL dissolution. Further research (here and elsewhere) is required to quantify the values of k_{B1}, and k_1, which are complex functions of hydrodynamics, microbial kinetics, and microbial accumulation.

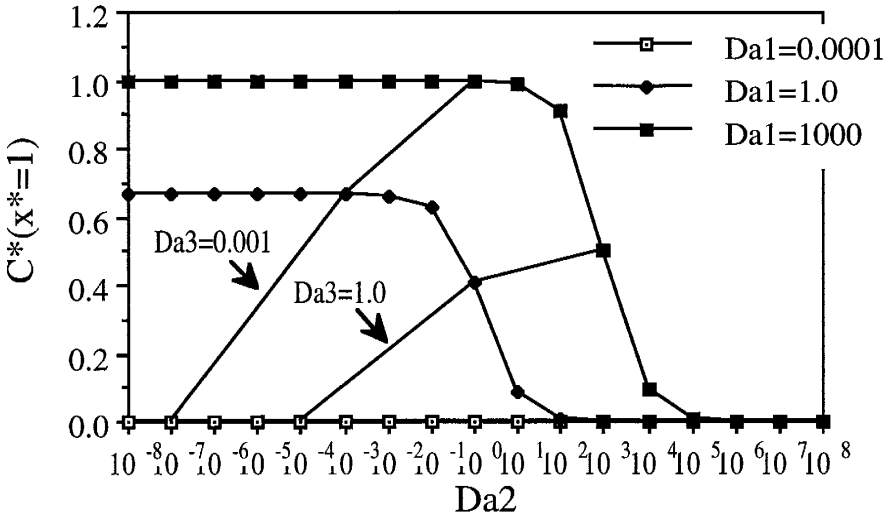

Figure 1 Representative curves (Pe = 1) showing how $C^*(x^* = 1)$ depends on Da_1, Da_2, and Da_3.

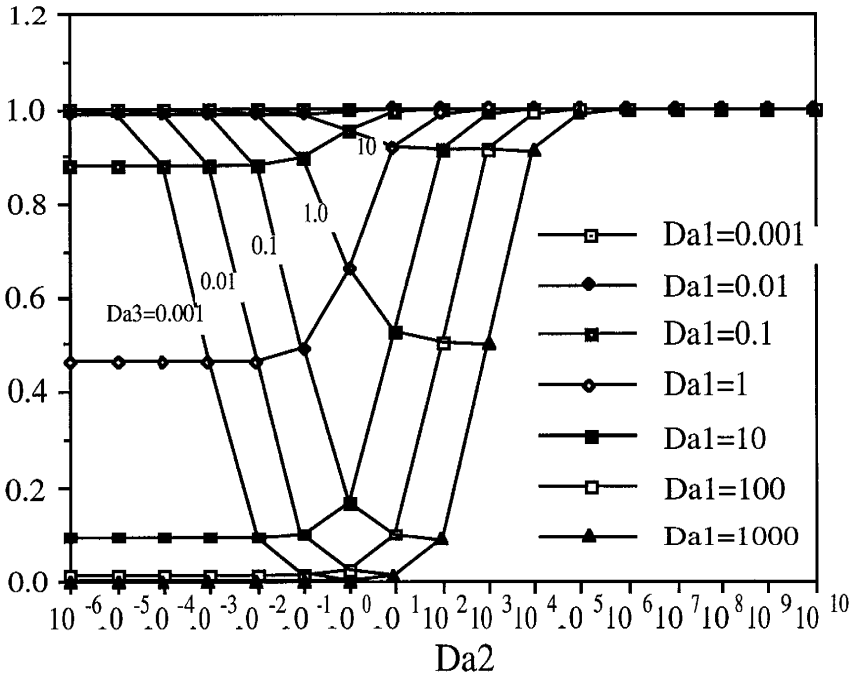

Figure 2 Representative curves of the normalized dissolution rate, rd^*, for a range of Da_2.

NAPL-Pool Dissolution in a Two-Dimensional Domain

10. A similar modeling analysis was carried out for a NAPL pool dissolving in a two-dimensional domain. The governing equation in the flowing liquid is

$$V_x \frac{\partial C}{\partial x} = D_z \frac{\partial}{\partial}\left(\frac{\partial C}{\partial z}\right) - k_{B1}C \quad (11)$$

in which z = the distance dimension normal to the flow direction [L] and D_Z = the transverse dispersion coefficient [L^2T^{-1}]. Equation 11 is nondimensionalized to

$$\frac{\partial C^*}{\partial x^*} = \frac{1}{Pe_t}\frac{\partial}{\partial}\left(\frac{\partial C^*}{\partial z^*}\right) - Da_2 C^* \quad (12)$$

in which Pe_t = a transverse Peclet number $=q_x L_X / D_Z$, and $z^* = z/L_X$. Interphase equilibrium is assumed for the boundary condition at the NAPL-aqueous phase interface,

$$C^*(x^*, z^* = 0) = 1 \quad (13)$$

for the entire domain, i.e., $0 \leq x^* \leq 1$. Solution of equation 11 gives the dimensionless solute concentration at any point in the domain (C^* (x^*, z^*)) and the total dimensionless dissolution flux, J^*, which is converted to the actual flux (J) by multiplying it by $V_X C_S$ (Seagren et al., 1994a).

11. Figure 3 summarizes the results very succinctly. The figure plots the enhancement factor E, which equals the dissolution flux with biodegradation divided by the dissolution flux with no biodegradation (i.e., $k_{B1} = 0$). For $Da_2 \leq 0.1$, biodegradation is insignificant and does not increase J. When Da_2 is or can be made greater than 0.1, biodegradation significantly accelerates dissolution. A strategy for increasing Da_2 is to increase k_{B1}, by increasing the amount of active biomass and/or by increasing the kinetics of the biomass by alleviating a limitation (e.g., electron acceptor) or improving environmental conditions (e.g., pH).

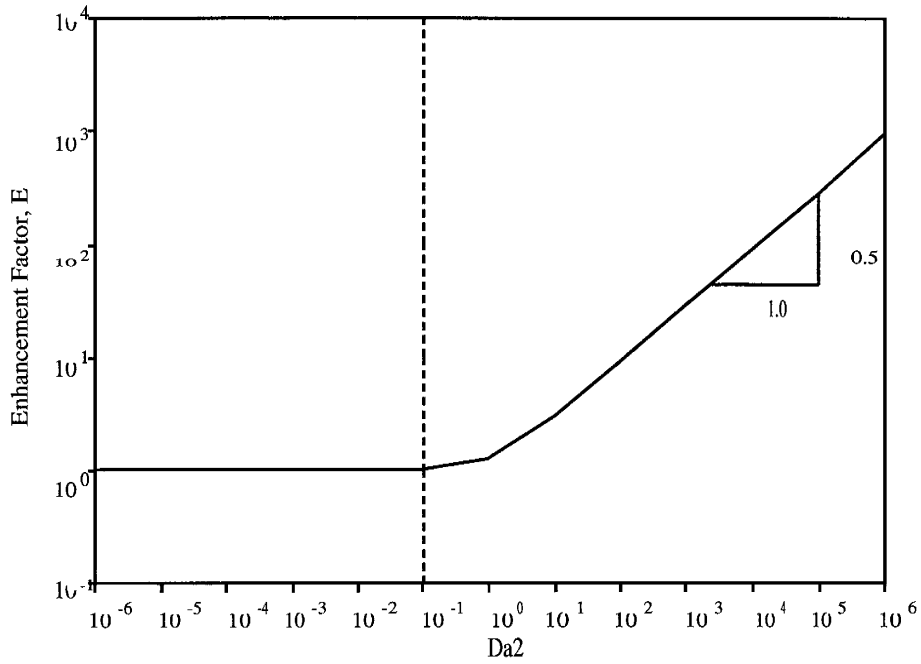

16. **Figure 3** Log E (=$J_{biotic}/J_{abiotic}$) for a range of Da_2.

Experiments

12. A series of experiments was carried out in a laboratory-scale porous-medium reactor in which dissolution from a NAPL pool could be carefully measured. The predicted effects of flushing and biodegradation were evaluated in abiotic and biotic experiments in which the toluene content of the pool and the water flow velocity were systematically varied.

13. Figure 4 shows that experimental system. Two reactors were used. The reactors were approximately 40-cm long borosilicate-glass columns with square (4.5 cm) cross-section. They were packed with 2-mm glass beads. Sampling ports, installed every 4.5 cm, accept syringe needles that can penetrate to different depths. Water flows from left to right, and the flow velocity is variable from 0.1 to greater than 10 m/day. The NAPL source is a small pool located in a reservoir 2 times the vertical width downstream from the inlet and extending one vertical width downstream.

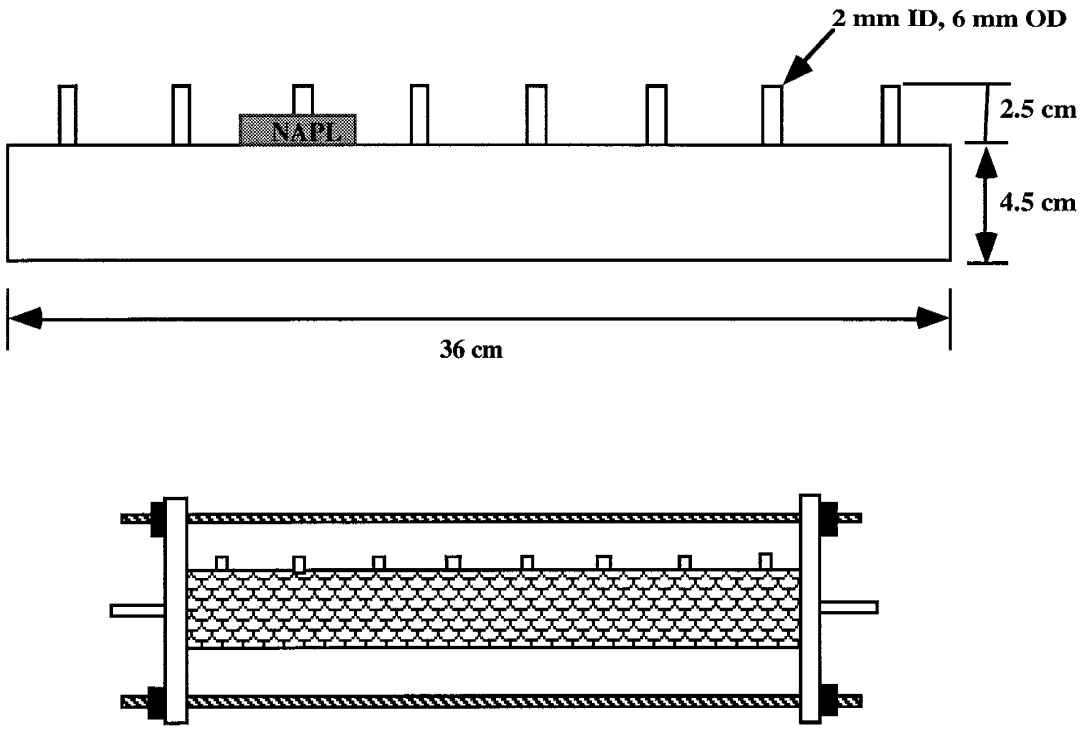

Figure 4 Schematic of the column design for the NAPL-dissolution experiments

14. Initial non-reactive tracer experiments were performed to characterize the reactors in terms of porosity, n, longitudinal velocity, a_X, and transverse dispersivity, a_Z. Reasonable values were obtained: For R1, n = 0.389, a_X = 0.210 cm, and a_Z = 0.00420 cm; and for R2, n = 0.389, a_X = 0.300 cm, and a_Z = 0.00310 cm.

15. Three model NAPLs were used in the experimental investigation: (1) neat toluene, (2) toluene at a mole fraction of $X_{tol} = 1.94 \times 10^{-2}$ in dodecane, and (3) toluene at a mole fraction of $X_{tol} = 8.76 \times 10^{-2}$ in dodecane. When it was necessary to visually distinguish the NAPL phase form the aqueous phase, the model NAPLs were dyed with the hydrophobic dye Oil Red O at 0.1 g/l. In all dissolution experiments, the focus was on dissolution of the toluene. Toluene was selected for use as the primary NAPL of study because: It is a representative of the groups of gasoline components most likely to partition in to water; it is an important groundwater contaminant; it can serve as a sole carbon and energy source for bacteria; and its solubility is sufficient that bacteria require

no special uptake mechanism. n-Dodecane (solubility = 0.0037 mg/l at 25° C (Verschueren, 1983)), was selected as the second component in the two component NAPL mixtures because it is representative of the gasoline hydrocarbon group that is least likely to partition into the water phase.

16. A series of abiotic experiments evaluated whether or not changes in the advective velocity controlled the dissolution rate as predicted by eqn. 11, with $k_{B1} = 0$. At steady-state, the dissolution rate of toluene from the pool equals the mass flow rate of toluene out of the reactor; therefore, the toluene dissolution rate was calculated by multiplying the quasi-steady-state effluent concentration by the average flow rate. The toluene dissolution flux averaged over the entire projected planar pool area was calculated by dividing the toluene dissolution rate by the total pool area. The results of the abiotic experiment are summarized in Figure 5, along with the model prediction made using independently estimated values for the system parameters. The data demonstrate the expected trend of increasing J as V_X increased. The model of eqn. 11 with the equilibrium boundary condition describes the data reasonably well for most of the range of V_X studied, particularly for $V_X < 10$ m/d.

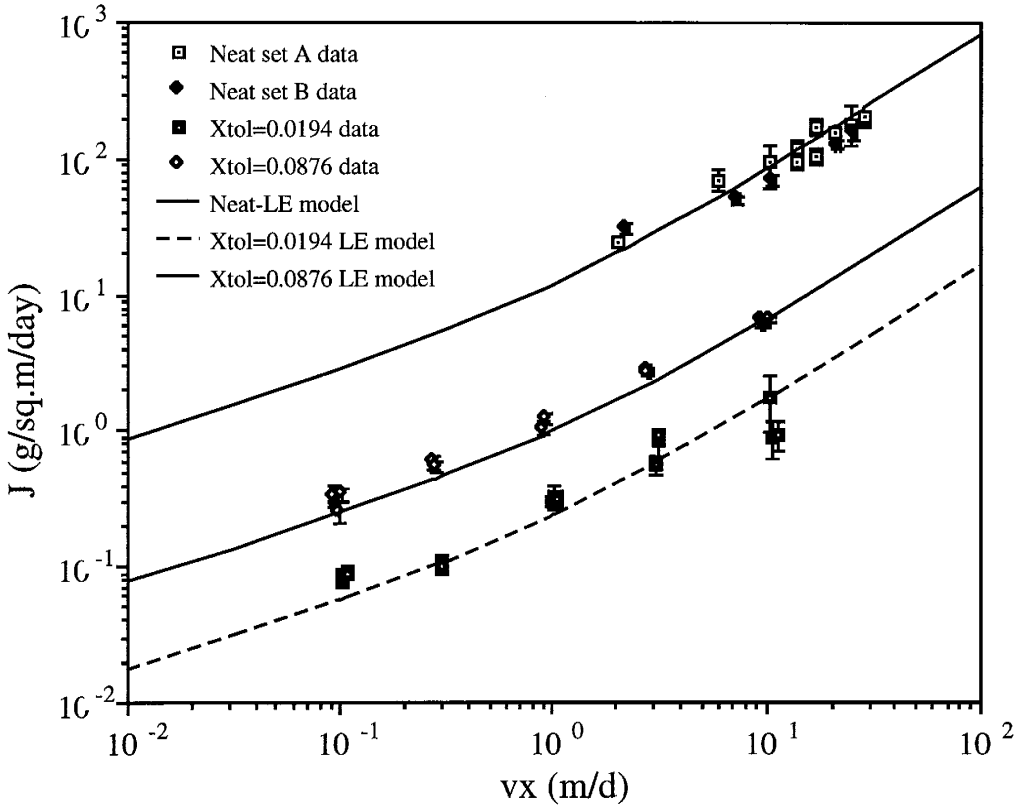

Figure 5 Summary of the experimental toluene dissolution flux results versus V_x for the three pool conditions studied -- pure toluene, $X_{tol} = 1.94 \times 10^{-2}$, and $X_{tol} = 8.76 \times 10^{-2}$.

17. Biotic experiments were carried out after the column had been inoculated with *Pseudomonas putida* PpG9, which oxidizes toluene. When a toluene-containing NAPL contacts water, non inhibitory conditions occur when toluene constitutes only a fraction of the NAPL and/or when the dissolved concentration is reduced by advection, dispersion, or degradation. In our preliminary experiments, bacterial growth and toluene biodegradation occurred only when the toluene concentration was less than the thermodynamic equilibrium concentration. Complete inhibition occurred when pure liquid toluene was in contact with the liquid.

18. In the biotic experiment, two flow velocities (0.1 and 1.0 m/d) and two binary toluene in dodecane NAPL mixtures ($X_{tol} = 1.94 \times 10^{-2}$ in dodecane and $X_{tol} = 8.76 \times 10^{-2}$ in dodecane) were used. We expected that biodegradation would have the greatest

impacts for the lowest velocity and the lower toluene content. For high flow velocity, advection is a major competing sink, and the relative effects of toluene biodegradation are small. Because the higher toluene content is large enough to cause toxicity, we expected to see a relatively larger impact for the experiments in which the toluene content was lower.

19. In these experiments, the NAPL pools were made using a stock ^{14}C-toluene solution to trace the fate of toluene and its biodegradation products. Samples in the effluent were assayed for the total, particulate, CO_2 and soluble volatile and nonvolatile organic ^{14}C. Based on a steady-state mass balance on the carbon in the System, the mass rate $[MsT^{-1}]$ of carbon out of the column (in the form of labeled $C0_2$, biomass, toluene, and soluble microbial products) must equal the mass rate of carbon (in the form of toluene) into the column from the pool. Therefore, the total ^{14}C activity during the quasi-steady-state period was used to calculate the carbon (i.e., toluene) dissolution rate from the pool by multiplying the ^{14}C total effluent concentration by the average flow rate. The toluene dissolution flux averaged over the entire projected pool area was calculated by dividing the toluene dissolution rate by the total pool area. A bacterial inhibitor (3 mM sodium azide) was added periodically to suspend the biodegradation sink and observe the abiotic dissolution rate for the same physical conditions.

20. The general trends were similar for all flow velocities and toluene concentrations, but important details differ. Figure 6 illustrates the general trends for the reactor in contact with the NAPL pool containing the lower toluene fraction (C_s = 11.3 mg/l, X_{tol}=0.02) and a flow velocity of 1 m/day. A quasi-steady state was reached between 30 and 50 hours, which correspond to 3 to 5 pore volumes. The steady-state dissolution flux can be computed from the total ^{14}C line and was 8.4 x 10^7 dpm/m^2-day. Of the total flux, approximately 50% was CO_2 produced from toluene mineralization. Another approximately 30% was radiolabelled biomass. Thus, only about 20% of the existing ^{14}C could have been from toluene or its breakdown intermediates.

21. The sodium azide inhibitor was added at 50 hours. Subsequently, the dissolution flux dropped to 4.8 x 107 dpm/m2-days, a value only 55% of the uninhibited flux. Furthermore, ^{14}C in CO_2 and biomass declined to close to zero. Clearly, the inhibitor had nearly stopped all biodegradation, which also caused a dramatic reduction in the dissolution rate.

22. At 64 hours, the inhibitor was removed from the feed. Although the experiment was stopped before a true steady state was re-established, the restoration of the higher dissolution rate with resumed biodegradative activity was clear.

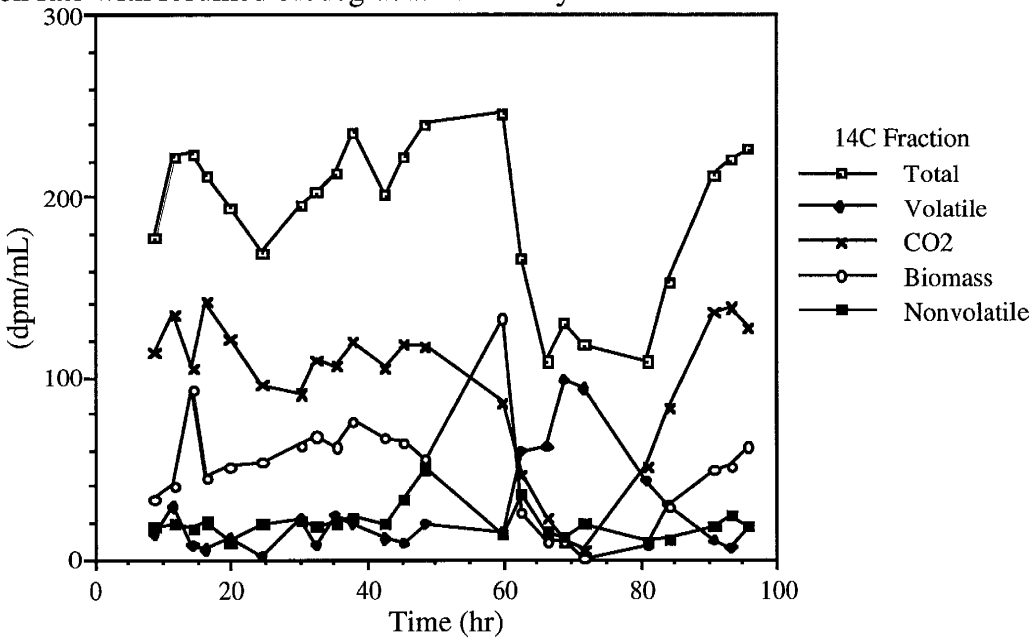

Figure 6 Fate of ^{14}C for the reactor in contact with the lower toluene fraction (C^*_S= 11.3 mg/l) and a flow velocity of 1m/day.

23. The data from the biotic experiments are summarized in Table 2. For easier comparison, the fluxes have been converted to (g/m^2 d) toluene using the specific activity of the toluene. The experimental results at $V_X \approx 0.1$ m/d and those at $V_X \approx 1$ m/d have been rearranged in the order of decreasing bioenhancement.

24. On the basis of the modeling work explained earlier, the magnitude of the bioenhancement affect should depend on the magnitudes of the solute concentration, the biomass concentration, the kinetic coefficients, and competing solute sinks. These factors

are explored sequentially using the modeling tools developed earlier. The assumptions of the biotic model preclude it being used quantitatively to analyze the biotic data because of violations of the model assumptions; however, it still can be used as a simple diagnostic toll, keeping aware of these liabilities.

Table 2 Summarized results of the biotic dissolution rate studies

Exp.	V_X (m/d)	C_S (mg/L)	J_{inhib} (g/m^2d)	J_{biotic} (g/m^2d)	J_{biotic}/J_{inhib}	$K_{B1eff.}$ (1/d)	q_{max}/K (L/mg d)
R1,set 1	0.104	5.08	0.0267	0.0501	1.88	7.85	0.0107
R1, set 2B	0.104	9.91	0.0521	0.0712	1.37	2.83	0.00386
R1, set 2A	0.101	10.89	0.0563	0.0654	1.16	1.14	0.00155
R2, set 2B	0.102	50.1	0.245	0.282	1.15	0.99	0.00589
R2, set 2A	0.102	53.2	0.260	0.222	0.85	[a]0	-
R1, set 2	0.954	11.81	0.269	0.465	1.73	57.3	0.0781
R2, set 2	0.919	92.5	1.77	1.86	1.05	2.9	0.0173

25. In the absence of toxicity, increasing the solute concentration should have a positive or neutral effect on the biodegradation solute sink, depending on the kinetic relationship. However, toluene is a self-inhibitory substrate for PpG9; therefore, increasing solute concentration may actually reduce the solute biodegradation sink. To estimate the solute concentration that the microorganisms in the primary zone of biological activity directly under and downstream of the pool experienced under the various experimental conditions, the values for J_{inhib} and the experimentally determined transport parameters were used with the abiotic local equilibrium (LE) model (governing equation is given by eqn. 11) to solve for the interfacial toluene equilibrium concentration. These values are summarized in third column of Table 2. There is a definite trend for increasing bioenhancement with decreasing estimated interfacial toluene equilibrium concentration. This strongly suggests that a toxicity effect was responsible for much of the observed variation in bioenhancement.

26. An "effective" value of the lumped first order biodegradation coefficient, K_{B1}, was calculated from the data by using J_{biotic}, the best-fit transport parameters, the fit value for C_S, and the biotic LE model. These values represent the combined effects of the effective kinetic parameters and the biomass concentration for each experiment and are summarized in the seventh column of Table 9. 17. As expected, the effective K_{B1} values are positively correlated with increasing bioenhancement effect. The effective K_{B1} values are inversely correlated with the best fit Cs. Therefore, the interfacial toluene equilibrium concentration appears to be an important factor for explaining the observed trends in bioenhancement, as reflected in the observed $J_{biotic}/J_{inhibited}$ ratio and calculated effective K_{B1} values.

27. The eighth column of Table 2 summarizes the computed q_{max}/K values which were computed as K_{B1} $n/X_f L_f a$. In general, q_{max}/K also declined with increasing Cs. This trend further supports the role of toxicity in decreasing the intrinsic kinetics for toluene degradation and biomass growth.

28. It was anticipated that the magnitude of the competing advection solute sink would also be an important factor in the magnitude of the bioenhancement effect. Unfortunately, because of the differences in C_S amongst the biotic dissolution experiments, and the resulting apparent toxicity effect, there are not enough data with all conditions the same except for v_X to draw any definite conclusions.

Conclusions

29. These experimental and modeling results demonstrate the enhancement of NAPL pool dissolution by flushing and biodegradation. In the absence of biological activity, flushing can increase the dissolution flux, but the magnitude of the impact depends on Pe_t. The NAPL dissolution model assuming local equilibrium at the NAPL-water interface gives reasonable predictions of the experimental dissolution flux results.

30. The biotic experimental results demonstrated the phenomenon of bioenhancement of the toluene dissolution flux, with the degree of enhancement dependent upon the

experimental conditions. In the experiments with the low toluene mole fraction (approximately 0.02), the presence of biological activity caused a statistically significant increase in the carbon dissolution flux at average pore water velocities of approximately 0.1 and 1 m/d; however, in all the experiments with the high toluene mole fraction of approximately 0.09, bioenhancement was either not observed or was statistically insignificant. Measurements of the biomass accumulation on the glass beads and analyses using the pool model suggested that high toluene concentrations caused a toxicity effect that was responsible for much of the observed variation in bioenhancement.

Paragraphs 1-2, Seagren et al., 1994b.
Paragraphs 3-22, Rittmann et al., 1993.
Paragraphs 23-30, Seagren 1994.

References

Bedient, P.B. 1991. NAPLs in the subsurface--a challenge for the 90s. Res. J. Water Pollut. Control Fed. 63:195

Mercer, J.W. and Cohen, R.M. 1990. A review of immiscible fluids in the subsurface: Properties, models, characterization and remediation. J. Contam. Hydrol. 6:107-163.

Rittmann, B.E. and Valocchi, A.J. 1993. Fundamental Quantitative Analysis of Microbial Activity in Aquifer Bioreclamation. Final Report.

Seagren, E.A., B.E. Rittmann, and A.J. Valocchi. 1993. Quantitative evaluation of flushing and biodegradation for enhancing *in situ* dissolution of nonaqueous phase liquids. J. Contam. Hydrol. 12:103-132.

Seagren, E.A. 1994. Biodegradation of Poorly Soluble Organic Contaminant. Unpublished thesis.

Seagren, E.A., B.E. Rittmannn, and A.J. Valocchi. 1994a. Quantitative evaluation of the enhancement of NAPL-pool dissolution by flushing and biodegradation. Environ. Sci. Technol. 28:833-839.

Seagren, E.A., B.E. Rittmannn, and A.J. Valocchi. 1994b. Comparative Abilities of Flushing and *in situ* Biodegradation to Accelerate NAPL Dissolution. Abstract, WEF conference.

Verschueren, K. 1983. Handbook of Environmental Data on Organic Chemicals, 2nd ed., Nostrand Reinhold Co., New York.

2. Micromodel Manufacture

preparing a pattern

A micromodels is composed of a pore network that is attached to reservoirs with inlets and outlets. The drawing of the micromodels pattern is created using Mathematica. The final printout is made on acetate at 2500 dpi at Subia in Albuquerque. This printout is then taken to a photographer, Bill DeMarco, so that a contact printing can be made. Contact printing gets rid of the need to use optics to reduce the image, which can cause line widths to become narrower and unexposable. This method of printouts is done so that you have two acetate printouts with emulsions on either side. The exposure step works best with emulsion to emulsion contact. The pattern must be greater than 11 cm between outlets so that microscope objectives can be changed without disturbing the model's tubing.

removing mirror backing

Mirrors can be bought with the backing already removed. These mirrors are more expensive and with the copper already exposed they are more susceptible to injury so that they cannot be used.

5" x 8" glass mirrors with a thickness of 3/8" were purchased from Ace Glass in Albuquerque. The enamel backing of the mirror must be removed to expose the copper. The stripping solution used for this is a mixture of ~95% dichloromethane (methylene chloride) and ~5% formic acid. The stripping solution is placed in a glass pan larger than a mirror. A mirror is placed in the solution with the backing face up. When the backing peels off the mirror, the mirror is removed from solution and rinsed with cold water. The mirror is rinsed with toluene, rinsed again with water and then washed with warm soapy water. The mirror is then quickly dried with compressed air. The stripped mirrors should be kept very clean.

With the backing removed, check the copper layer. Keep only unblemished mirrors.

coating the mirror

The mirror is coated with Kodak thin film resist (KTFR) supplied by Photofabrication Chemical and Equipment Co. This must be done in a dark room. A mixture of 3:1 xylenes:KTFR is used. The coating is applied at one end of the mirror and the mirror is then tipped so that the KTFR coats the entire mirror. The mirror is tipped back and excess coating is poured off. The mirror is then placed on end to dry. The end which the excess was poured off is to be placed at the bottom. The excess coating is saved for later steps.

Care should be taken to avoid coating the mirror too thickly. The coating is too thick when striations can be seen when the mirror is looked under a light.

The coated mirror should be allowed to air dry in a dark place for several hours. Allowing the mirrors to cure for 2-3 days can make them easier to expose.

exposure

This step is the most difficult to master. The exposure time varies and there are many places where errors can occur.

In a dark room, put the emulsion-side of the pattern transparency on the coated side of a mirror. Place a clear glass plate on top of the transparency to insure good contact and minimal light leakage. Put the plate and transparency under an ultraviolet light source for exposure of the KTFR. Exposure to ultraviolet light hardens the KTFR. Exposure time varies from 1.5 to 5 minutes depending on resist thickness, light source intensity and distance and pore size. Longer exposure reduces the fine detail, thicker resist needs longer exposure. The exposure time needs to be determined experimentally each time. If

the plate is underexposed, the resist will wash off in the next step. Overexposure causes the pattern to lose details and pore connections.

The light source is four 15W black light blue light rods that are 30 cm away from the mirror with two diffusers in between to even out the light. The first diffuser is 20 cm above the mirror with the second 4 cm above that. The mirror is enclosed in a box constructed of matte black poster board to eliminate light bleeding under the pattern. Exposure times are generally around two minutes.

development

When the exposure is complete and the room light is still dim, hold the mirror horizontally and spray xylene on the surface. The plate is tipped back and forth. Excess xylene is drained off. This can be repeated as often as needed. The xylene dissolves the undeveloped resist.

The mirror is then rinsed with warm tap water. The water must be at low flow, if the flow is too high all the resist will be washed off. This is especially important for very fine detailed patterns with short exposure times. The plate is dried with compressed air. Place the plate in concentrated nitric acid for 5 seconds, or until the unprotected copper and silver layers dissolve to reveal the underlying glass surface. The plate is rinsed quickly with cold tap water and dried again with compressed air. Water on a developed plate can cause the copper to dissolve.

Check the plates under a microscope and keep only the well-developed ones for the final models. It is useful to keep some almost good plates for the next step to determine etching times.

etching

All areas of the glass that need to be unetched, such as the model edges and back, are coated with resist. The resist to be used is the excess saved from the coating step. The

back should be coated twice so that scratches aren't etched in which can affect the final model's appearance.

After the plates are allowed to dry overnight, the plate is placed in a tray of concentrated HF acid. Longer etching times are used for models requiring deeper pores. The depth of the etching should be equal to the average throat width. To determine the necessary etching time, start at 10 minutes. If that is too short go to 20 minutes, and if necessary iterate between the two times. Don't go over 20 minutes. For the tiny micromodels, an etching time of only four to five minutes was needed. For larger ones, a time of 20 minutes was used.

When the plate is removed from the acid it is rinsed in cold water, and the network is scrubbed with a hard brush to remove silica deposits formed during etching. The resist is removed with a razor. The exposed copper and silver are then removed with nitric acid.

fusing

Inlet and outlet pores are drilled using a 1.5 mm diamond tipped drill bit on a drill press at low speed. The pores are drilled on only one side of a pair of plates. After drilling, the plates are washed with soapy water and brushed thoroughly. They are then placed into an ultrasonicator for 20 minutes for remove the fine silica. The two halves are aligned under a microscope and a small drop of silicone glue is added at the corners between the plates. The glue is allowed to dry. The model is then placed in a muffle furnace and fused at 705^{o}C for about 15 minutes. Higher temperatures and longer fusing times result in smoother smaller pores; however, when the temperature is too high and fusing time too long, pores will close and the network can become disconnected. A completed micromodel can be removed after the furnace is cooled to below 75^{o}C. Removal before then can cause the model to shatter.

tubing

Tubing is attached using fittings. Clamps are used which fit VCO Swagelok fittings. The fittings compress onto the model and leaks are prevented by an o-ring in the fittings. Teflon tubing is then attached using Swagelok compression fittings.

3. *Pseudomonas putida* PpG9: Literature Review

Pseudomonas putida PpG9 was isolated from soil. I received my cultures from the culture collection of I.C. Gunsalus at the University of Illinois, Urbana-Champaign. They got the bacteria from Nozaki who isolated it from soil in a benzoate enrichment. The bacterium was originally name *Pseudomonas arvilla* mt-2. It was later named *P putida (arvilla)* mt-2, and then became *P. putida* mt-2 before being named *P putida* PpG9.

This bacterium carries the TOL plasmid and can degrade aromatic hydrocarbons. Toluene degradation is a tightly regulated system with control at the level of transcription (Burlage et al., 1989).

The genes for the degradation of toluene are carried partly on the TOL plasmid and partly on the chromosomes (Vecht et al., 1988). The degradative pathway for toluene is shown in fig. 1. The genes code for *ortho* cleavage of the catechol while the plasmid codes for *meta* cleavage (Burlage et al., 1989). The TOL plasmid is transmissible. The TOL plasmid is usually found on *Pseudomonads* and related species.

P. putida can grow on toluene, p-xylene, m-xylene and their degradation intermediates: benzyl alcohol, p-methylbenzyl alcohol, m-methylbenzyl alcohol, benzalhdehyde, p-tolualdehyde, m-tolualdehyde, m-toluate and acetate (Worsey and Williams, 1975). It can grow with decane, hexane cyclohexane or pentane present in separate liquid phase. It cannot grow in the presence of 20% vol/vol liquid phase p-xylene, cyclopentane, toluene, 1-heptanol, or benzene (Cruden et al., 1992).

In batch studies, partial inhibition of growth of *P. putida* in 0.7 g/L m-toluic acid began at 0.3 g/L initial concentration of liquid toluene. Complete inhibition was observed at >1.4 g/L (Vecht et al., 1988). Toluene was found to inhibit initial growth and preliminary studies of Vecht showed no growth on liquid toluene. This may possibly be caused by cell damage due to liquid toluene.

Growth on vapor is inhibited at 0.36 g/L (Vecht et al., 1988). Vecht also performed chemostat studies and recovered 70% of the toluene in the airstream. Of the toluene that went into solution, 70% of it was converted to biomass. The specific growth rate was 0.14 hr^{-1}, which was comparable to the growth in batch studies.

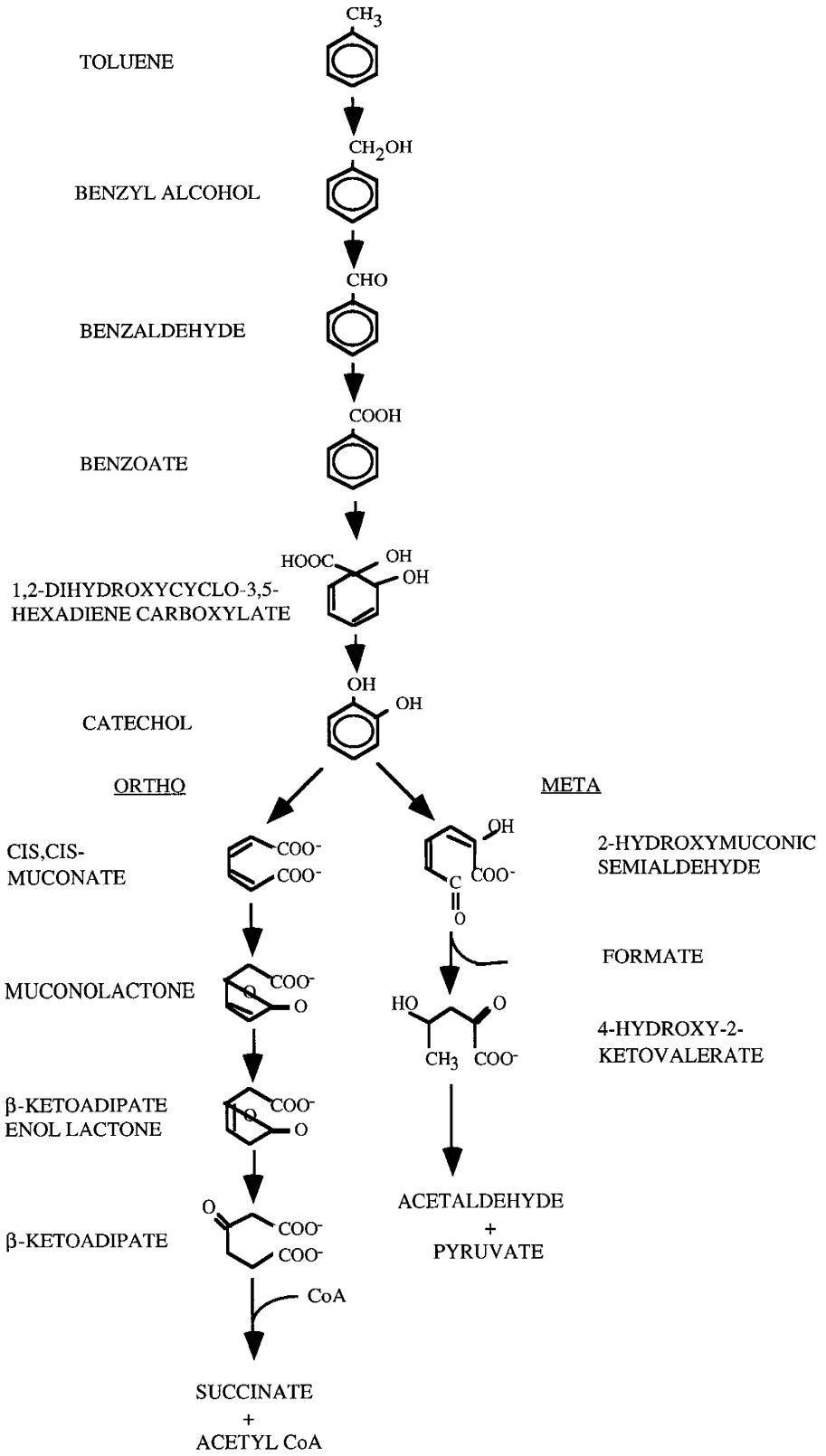

Figure 1 Pathway for toluene degradation. The meta pathway is coded for by the TOL plasmid. The ortho pathway is coded for on the chromosomes of *P putida*

References

Burlage, R.S., S.W. Hooper, G.S. Sayler. The TOL (pww0) Catabolic Plasmid. Applied and Env Microbiology. 55: 1323-1328. 1989.

Cruden, D.L., J.H. Wolfram, R.D. Rodgers, D.T. Gibson. Physiological Properties of a *Pseudomonas* Strain Which Grows With p-Xylene in a Two-Phase (Organic-Aqueous) Medium. Applied and Env. Microbiology. 58: 2723-2729. 1992

Vecht, S.E., M.W. Platt, Z. Er-El, J. Goldberg. The Growth of *Pseudomonas putida* on m-Toluic Acid and on Toluene in Batch and Chemostat Cultures. Applied and Env Microbiology. 27: 587-592. 1988

Worsey, M.J., P.A. Williams. Metabolism of Toluene and Xylenes by *Pseudomonas putida (arvilla)* mt-2: Evidence for a New Function of the TOL Plasmid. J. Bacteriology. 124:7- 13. 1975.

B. Appendix B

1. The Role of Growth Medium on Bacterial Hydrophobicity

Introduction

Bacterial adhesion plays an important role in daily life. From the proper functioning of agricultural soil and pipelines to dental cavities and biodegradation, the interaction between bacteria and interfaces supports important functions.

Bacteria exist as both free-living and attached cells (Ellwood et al., 1979). Physical, chemical and biological phenomena tend to concentrate water, substrates, metabolites, nutrients and microbes at surfaces. Consequently, microorganisms perform their important roles at the surfaces of solids and not while suspended. Nutrient and growth conditions can affect adhesive capabilities, but there is no general pattern (Fletcher, 1991).

Prospects for in-situ bioremediation of contaminated groundwater, microbially enhanced oil recovery and other subsurface bacterial processes have stimulated research on the fate and transport of microorganisms. These prospects have increased the demand for the ability to accurately predict the rate and extent of microbial transport through porous media. For bacterial sized spheres, surface chemical properties had a greater effect on retention than did size (Harvey et al., 1989)

The hydrophobicity of a bacteria's surface is often used to make predictions of the extent of microbial attachment to surfaces. These predictions are then often used in mathematical models. The discussion of the relation between hydrophobicity and binding affinity is relevant for its possible ecological significance (Kjelleberg and Hermansson, 1984).

Bacteria are generally thought to be hydrophobic. With the exception of a few strains, no microbes are so hydrophobic as to be wetted by oil and not by water. The inclination of bacteria to exhibit hydrophobicity is determined by interplay between polar and non-polar surface components (Loosdrecht et al., 1987). In bacteria without fimbriae

or fibrils, the hydrophobic proteins are uniformly distributed in a layer over the cell surface (Paul and Jeffrey, 1985).

One way to determine cell surface hydrophobicity is through the use of contact angles. Contact angles provide an important factor for predicting a cell's adhesion to various surfaces (Loosdrecht et al., 1987). Microbial adhesion to hydrocarbon MATH assay has been most frequently studied during the past decade as another measure of cell surface hydrophobicity (Rosenberg, 1991).

Methods

The contact angles were measured using the thick smear technique (Aaron Mills, personal communication). *Pseudomonas putida* PpG9 were grown in a liquid medium until the suspension was very turbid (approximately 72 h). Two liquid media were used, 10% PTYG and mineral medium (table 1) with toluene vapor. The media were inoculated from cultures grown on plates of either TSA or mineral medium with toluene vapor so that four growth regimes (tol:tol, tol:PTYG, TSA:tol, and TSA:PTYG) were established. The suspension was then washed in artificial groundwater (AGW) (table 2) and resuspended in AGW for 24 - 48 hours. The cells were then centrifuged at 12,100 x g for 10 minutes. The supernatant was removed and the centrifuge tube was placed on its side with the pellet facing up, so as not to rewet the pellet. A sterile inoculating loop was then used to smear the bacteria thickly onto a clean glass slide. This smear was allowed to dry in a dessicator for approximately 4 hours prior to contact angle measurements. A single drop of distilled water was placed on the smear with a nanoliter pipette. Using a Zeiss microscope with a goniometer eyepiece, measurements were made on both sides of the drop after it had stabilized. Measurements were made in several spots on each smear.

The MATH assay was performed with washed bacteria also resuspended in AGW. 5.0 ml of the turbid suspension was added to an acid-washed cuvette, 1.0 ml of oil paraffin (oil petrolatum, Central Scientific Co.) was then added on top. Oil paraffin is a mineral oil. Absorbance was measured at 680 nm using a Spectronic 20 (Milton Roy

Co.). The cuvettes were then covered and vortexed for 1 minute. The oil paraffin was then allowed to recoalesce (at least 30 minutes) and absorbance measurements were made again. An increment of 1 ml of oil paraffin was added. The mixture was then vortexed for 0.5 min. and absorbance was re-measured. This was done until absorbance measurements reached steady-state.

The MATH assay was not performed with toluene as it causes cell lysis.

Mineral Medium		10% PTYG	
Compound	g/L	Compound	g/L
KH_2PO_4	2.04	glucose	1.0
Na_2HPO_4	2.13	yeast extract	1.0
$(NH_4)_2SO_4$	1.0	peptone	0.5
$CaCl_2 \cdot 2H_2O$	0.0110	trypticase	0.5
$MgSO_4 \cdot 7H_2O$	0.20	$MgSO_4 \cdot 7H_2O$	0.6
$FeSO_4 \cdot 7H_2O$	0.007	$CaCl_2 \cdot 2H_2O$	0.07
$ZnSO_4 \cdot H_2O$	0.002		
$MnSO_4 \cdot H_2O$	0.00154		
$CuCl_2$	0.00021		
$CoCl_2 \cdot 6H_2O$	0.000404		
H_3BO_3	0.00011		
$Na_2MoO_4 \cdot 2H_2O$	0.00025		
H_2SO_4 (conc.)	few drop to pH=6.8		

Table 1 Composition of mineral media. Agar plates included 40g/l agar (Difco).

AGW	
1.5*10^-5M	KNO_3
1.4*10^-4M	$MgSO_4 \cdot 7H_2O$
7.0*10^-5M	$CaSO_4 \cdot 2H_2O$
8.0*10^-5M	NaCl
1.4*10^-4M	$NaHCO_3$

Table 2 Composition of AGW.

Results and Discussion

The hydrophobicity of *Pseudomonas putida* varied depending on growth media. The contact angles of the four growth regimes showed that bacteria grown on liquid mineral media with toluene vapor were more hydrophilic than bacteria grown on 10%

PTYG broth (figure 1). The contact angles for the bacteria grown in mineral medium broth with toluene vapors had contact angle measurements in the low 30's. The cells grown on PTYG broth had contact angles in the 60's. This indicates that the 10% PTYG bacteria will have greater adherence to surfaces.

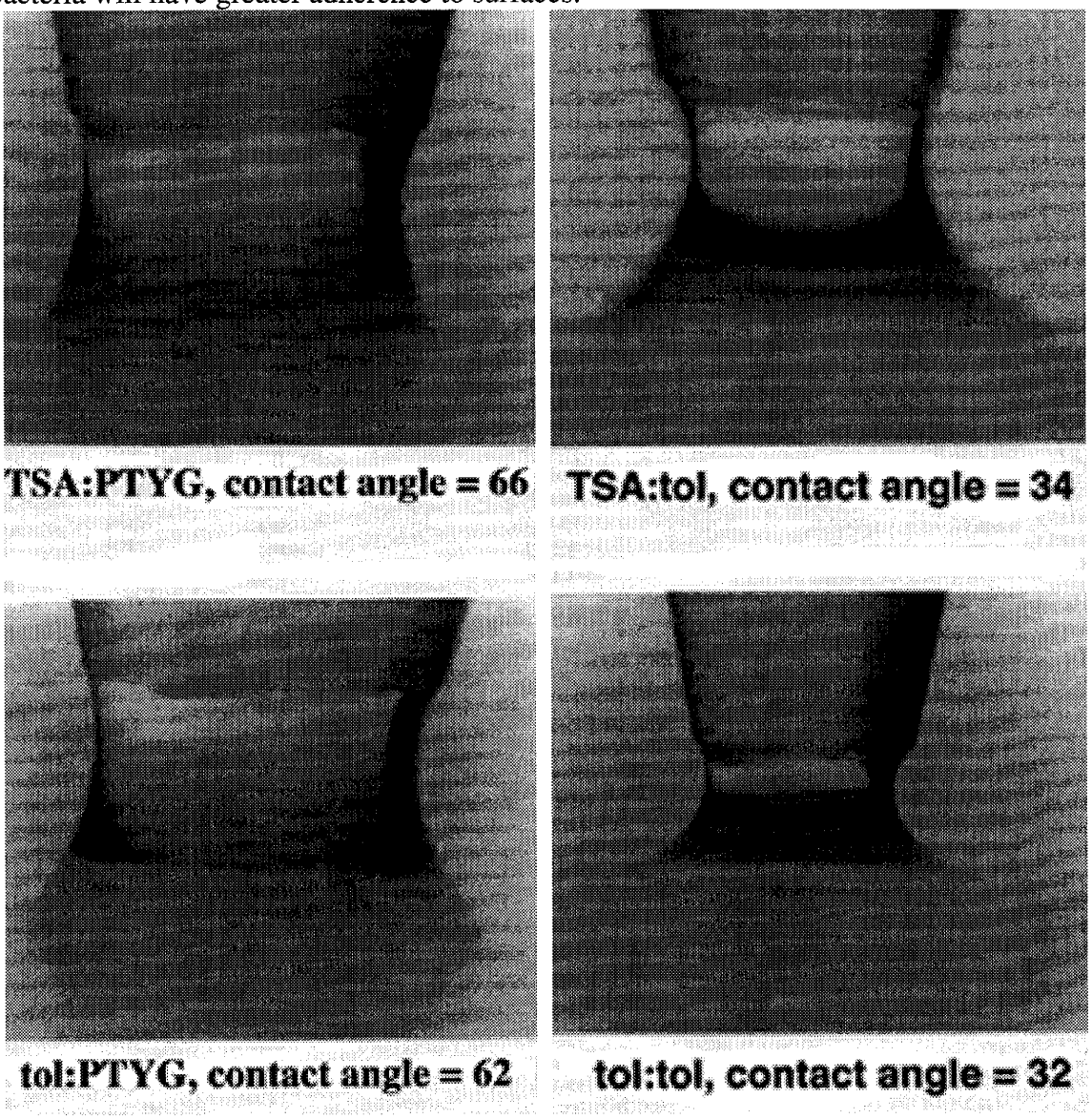

Figure 1 Contact Angles Pictures and measurements of the four growth regimes.

The MATH assay results are contrary to that prediction (figure 2). They showed a greater absorbance into the hydrocarbon phase by bacteria grown on mineral medium with toluene vapors. This correlates with Singh and Vincent (1987) who showed that

bacteria growing in a dilute medium were hydrophobic as determined by a MATH assay. Bacteria grown in a rich nutrient broth were not.

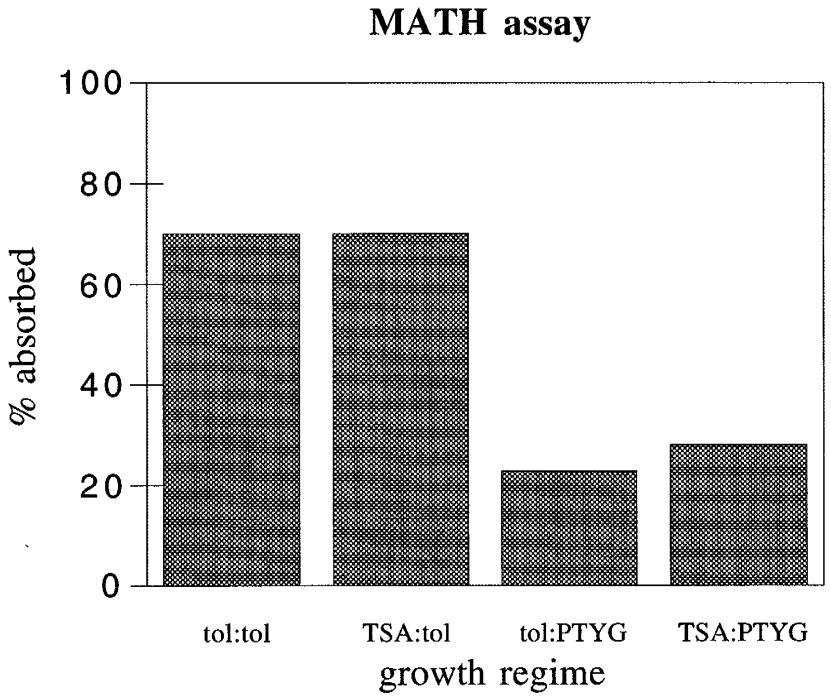

Figure 2 MATH Assay Results Growth regime is one of the four regimes described above. The percent absorbed is the percent loss in reading at 680 nm.

Not all bacteria behave as expected from contact angle measurements (Loosdrecht et al., 1987). This indicates that interactions other than hydrophobicity may also play a role in bacterial partitioning.

The mineral medium had higher ionic strength (I=0.086) then the 10% PTYG (I=0.01). Bacterial adhesion increases with increasing ionic strength (Scholl et al., 1990). This can be predicted from the DLVO theory. Since the bacteria are all washed, resuspended and allowed to come to rest in the same media (AGW), the ionic strengths of the growth media plays no role in the bacteria's adhesive abilities.

Adhesion is an active process involving cell metabolism (Caldwell and Lawrence, 1986), and is sensitive to the time allowed for contact with a surface (Scholl et al., 1990).

The MATH assay has no definitive method. Adhesion, as measured by the this assay, is sensitive not only to time allowed for vortexing, but also to the amount of surface area created during mixing of the two liquid phases (Loosdrecht et al., 1987).

Conclusions

Growth medium affects the hydrophobicity of bacteria cell surfaces. The change is dependent upon the last medium the bacteria was grown in and not on previous culture media. This should be taken into account when using measures of hydrophobicity (contact angles, MATH assay) to predict fate and transport of bacteria in the subsurface. Microorganisms are often genetically altered during the process of purification and consequently the acitivity of lab cultures sometimes misrepresent the activity of natural populations (Caldwell and Lawrence, 1988).

Microorganisms adapt genetically and thus change their intrinsic properties as they are studied (Caldwell and Lawrence, 1988). They are able to maintain their options so that they can vary their attributes in response to environmental factors. Consequently, most of the cells we refer to as being hydrophobic appear to be simultaneously hydrophobic and hydrophilic (Rosenberg, 1991). They can also produce progeny with different surface chemistries which can take advantage of whatever environmental circumstances present themselves (Fletcher, 1991). This is one explanation for why the hydrophobicity varies with different growth media.

In order to get maximum benefit out of the microcosm they are in, bacteria must respond to environmental factors quickly. The external configuration of the cell surface components of dynamically hydrophobic strains can undergo dramatic changes (Rosenberg, 1991). The bacterial populations from this study exhibited dynamic hydrophobicity. Due to this, cells in the aqueous phase assume configurations that maximize interactions with water. But when in contact with surfaces, different, more hydrophobic structures are assumed. This dynamic hydrophobicity is a function of environmental stresses placed upon bacteria.

References

Caldwell, D.E., J.R. Lawrence. 1988. Study of Attached Cells in Continuous-Flow Slide Culture. In J.W.T. Wimpenny Ed. Handbook of Laboratory Model Systems for Microbial Ecosystems Volume 1. pp117-138. CRC Press, Boca Raton, FL.

Caldwell, D.E., J.R. Lawrence. 1986. Growth Kinetics of *Pseudomonas fluorescens* Microcolonies within the Hydrodynamic Boundary Layers of Surface Microenvironments. Microb Ecol 12:299-312.

Ellwood, D.C., J. Melling, P.Rutter, Ed. 1979. Adhesion of Microorganisms to Surfaces. Academic Press, NY.

Fletcher, M. 1991. Bacterial Colonization of Solid Surfaces in Subsurface Environments. In C.B. Fliermans, T.C. Hazen (Eds), *Proceedings of the First International Symposium on Microbiology of the Deep Subsurface* (pp7-6-7-12). Aiken, SC: WRSC Information Services.

Harvey, R.W., L.H. George, R.L. Smith, D.R. LeBlanc. 1989. Transport of Microspheres and Indigenous Bacteria Through a Sandy Aquifer: Results of Natural- and Forced-Gradient Tracer Experiments. Environ Sci Technol. 23:51-56.

Kjelleberg, S., M. Hermansson. 1984. Starvation-Induced Effects on Bacterial Surface Characteristics. Appl Env Microbiol 48:497-503.

Loosdrecht, M.C.M., J. Lyklema, W. Norde, G. Schraa and A.J.B. Zehnder. 1987. The Role of Bacterial Cell Wall Hydrophobicity in Adhesion. Appl. Env. Microbiol. 53:1893-1897.

Paul, J.H., W.H. Jeffrey. 1985. Evidence for Separate Adhesion Mechanisms for Hydrophilic and Hydrophobic Surface in *Vibrio proteolytica*. Appl Env Microbiol. 50:431-437.

Rosenberg, M. 1991. Basic and Applied Aspects of Microbial Adhesion at the Hydrocarbon:Water Interface. Critical Reviews in Microbiol 18(2):159-173.

Scholl, M.A., A.L. Mills, J.S. Herman, G.M. Hornberger. 1990. The Influence of Mineralogy and Solution Chemistry on the Attachment of Bacteria to Representative Aquifer Materials. J Contaminant Hydrology 6:321-336.

Singh, K.V., W.S. Vincent. 1987. Clumping Characteristics and Hydrophobic Behaviour of an Isolated Bacterial Strain from Sewage Sludge. Appl Env Microbiol 25:396-398.

2. Comparison of Two Micromodel End Reservoirs

Introduction

Etched glass micromodels have been used to make detailed observations of interface movements since 1961 (Mattax and Kyte, 1961). Micromodels are used to see flow processes and are most often qualitative (Buckley, 1991). Buckley, 1991, states that although quantitative data is reported, it is of limited significance and the dangers of generalization from micromodel experiments cannot be over emphasized.

Despite this, Mattax and Kyte, 1961, noted that micromodels may be reasonable representatives of natural porous media. In Wardlaw and McKellar, 1981, mercury injection and withdrawal capillary pressure tests were done to identify aspects that affect trapping of non-wetting fluids. They concluded that threshold pressure anomalies may occur due to boundary effects. Since then, much work has been done to try to identify these boundary effects. Computer simulations were done which revealed that the boundary effects are at a maximum at breakthrough in drainage and that their maximum extent in 2-D models is a distance of about 40 pore throats. The effects of boundaries are important to understanding errors when small networks are used to represent large systems (Li, et al., 1986). The understanding of boundary and end effects are also useful because they are common experimental artifacts in displacements conducted in sample cores of reservoir rocks (McKellar and Wardlaw, 1982).

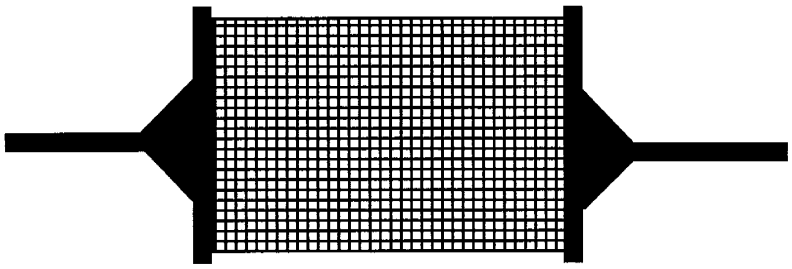

Figure 1 Example of an etched glass micromodel pattern

One of the easiest to see examples of end effects is the effect of the large reservoirs at the output of micromodels (fig 1). In columns, the effects of these reservoirs are mediated by their relatively small volume in comparison to the column pore volume. Due to the small volumes used in micromodels, their effects are amplified. These reservoirs lead to short, preferential flow paths.

A micromodels designed with branching at the end was compared to a standard end reservoir model (fig 2). The hypothesis is that branching eliminates the preferential flow paths and insures even mixing. These two effects combined should reduce the end effects so that breakthrough curve data would be more accurate.

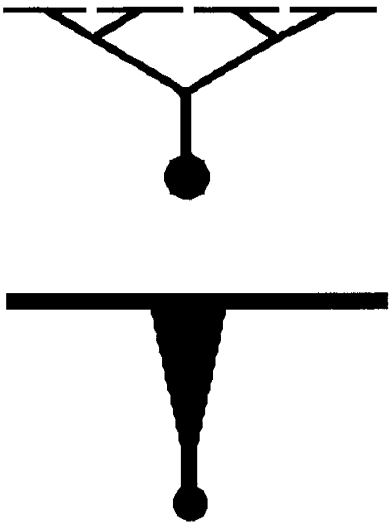

Figure 2 The two end reservoirs to be compared

Methods

Two micromodels were constructed according to Wan and Wilson, 1993. These micromodels were then cut with a rock saw so that 0.75 mm of the pattern was left before the end reservoir. The models were photographed using ESEM to determine pore sizes.

Using pieces of clear acrylic, cells were constructed so that the model was divided into four even sections. These cells were then epoxied onto the cut end of the micromodels (fig 3).

Water was injected into the cells. The far right cell was filled with dyed water while the others were filled with undyed water. Sequential outflow was collected for analysis by spectrophotometer for color intensity. The volume of water used is equal to the amount of water stored in the cells and tubing. No water was added after a cell

emptied. The water was forced through the model as it would be in a flow experiment. At least five trials were held.

The small model held 8 ml in the cells and tubing. The large model held 15 ml. At least four ml was needed for measurement by spectrophotometer. For this reason only two sequential samples were collected from the small model, while three were collected from the large model.

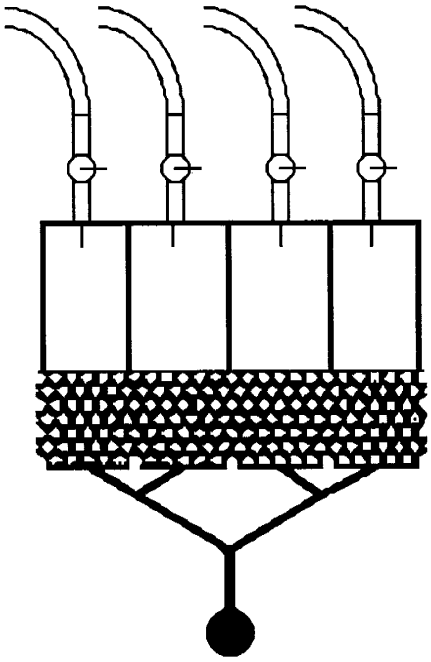

Figure 3 Schematic of micromodel with cells and tubing attached

Results and Discussion

The model with the single reservoir has larger pores, ranging in size from 500 - 1500 mm. The average pore size is approximately 1000 mm. The model held 0.42 ml of water in the pore space and reservoir. The other model has pore sizes ranging from 10 -

500 mm, the average being approximately 200 mm. The small model held 0.13 ml of water in the pore space and reservoir. During the experiments, 15 ml of water (35 pore volumes) of water was collected from the large model and 8 ml (61 pore volumes) was collected from the small model.

During sample collection, the single reservoir model had the middle two cells empty first. Although the water drained out of the tubing at the same rate initially, after the water level reached the cell structure, the outside two cells stopped flowing. The branching reservoir model's cells emptied more evenly. When the experiment initially started, the right cell would take a moment to get started.

Table 1 shows the transmittance readings of the sequential samples. The difference between the initial measurements and the measurements after the first cells started to empty is less with the small model with the branching. This indicates that the branching reservoir samples from all sections of the micromodel much more evenly than the single reservoir model.

model	1st collection	2nd collection	3rd collection
small	46.5	26.8	ND
large	70.2	70.5	19.8

Table 1 Transmittance of sequential collections.
All values are percentage transmittance as read at 600 nm. 100% transmittance was set using water as a blank. 0% transmittance was set using pure red water. A 3:1 mix of water to dyed water was read at 42%. All sample volumes were uniform.

Conclusion

It was shown that branching on the reservoir samples the micromodel uniformly. The standard single reservoir allows for fast flow paths through the middle of the model. This means that samples obtained from single reservoir models are not balanced samples of the entire flow domain and are samples of the center of the model. This would also indicate that branching exit reservoirs lessen the end effects.

When trying to establish breakthrough curves, it is important to sample the whole micromodel and not just the center. Because of this, it is important to use branching in your micromodel pattern. Single reservoir models would still be effective if you are only looking at flow in pores and are not concerned with end effects or breakthrough curves.

References

Buckley, Jill S. Multiphase Displacements in Micromodels. in Interfacial Phenomena in Petroleum Recovery edited by Norman R. Morrow. Marcel Dekker, Inc. New York. 1991.

Li, Yu, W. G. Laidlaw, and N.C. Wardlaw. Sensitivity of Drainage and Imbibition to Pore Structures as Revealed by Computer Simulation of Displacement Process. Advances in Colloid and Interface Science 26: 1-68,1986.

Mattax, C.C. and J.R. Kyte. Ever See a Water Flood? The Oil and Gas Journal, 59: 115-128, 1961.

McKellar, M, and N.C. Wardlaw. A Method of Making Two-Dimensional Glass Micromodels of Pore Systems. J. Canadian Pet Tech. 21: 39-41, July-August, 1982.

Wan, J. and J.L. Wilson. Visualization of the Role of the Gas-Water Interface on the Fate and Transport of Colloids in Porous Media. Water Resources Research. 30:11-23.

Wardlaw, N.C. and M. McKellar. Mercury Porosimetry and the Interpretations of Pore Geometry in Sedimentary Rocks and Artificial Models. Powder Technology, 29: 127-143, 1981.

C. Appendix C

1. A New Technique for Visualization of Bacteria in a Simulated Porous Medium

ABSTRACT

Bioremediation models make assumptions about the distribution and attachment of bacteria in the subsurface. A new method for viewing bacteria in a micromodel was developed to validate one of those assumptions.

Previous work required very simple flow configurations and/or destruction of the porous media to determine where the bacteria were distributed. This new technique allows complex inputs and outputs into the flow configuration without requiring destruction of the medium. This will allow the observation of the bacteria over time, as flow conditions change. It will also permit the micromodel to simulate more closely the actual conditions in a field site employing bioremediation.

The micromodel is used as a simulated porous medium. It is a 1/4" glass plate with a two dimensional pattern etched into the middle. Fluids can flow through it while an observer can see the interactions among the fluids and any introduced particles.

This procedure uses principles of fluorescence microscopy. It employs fluorescent bacterial stains that leave the cells viable. Also used is a series of filters that allow excitation of the stained bacteria but don't allow stray light to be transmitted. By construction of a laboratory apparatus, long focal lengths are allowed which permit the use of complex tubing placement and arrangement on the micromodel.

By using this new technique, I was able to observe the bacteria in a micromodel. I was also able to observe the flow paths of bacteria during a dynamic experiment.

Introduction

Bioremediation models make many assumptions about the distribution and attachment of bacteria in the subsurface. One of these assumptions may be that the bacteria will colonize a region along a contaminant plume where the chemical's concentration is favorable to their growth. This concentration will be such that the bacteria can use the contaminant as a food source but will not be so great that the chemical is toxic. In this way, the contaminant acts as a self-inhibiting substrate.

This assumption appears to be borne out by experimental evidence. Bacteria from a contaminated site showed no lag phase for benzene degradation when benzene was added at 1 mg/l (Davis et al., 1994). When the concentration was increased to 10 mg/l, a lag phase of ten days was observed. This indicates that the bacteria in the aquifer were acclimated to lower concentrations and that the bacteria are situated in the region where the concentration is low.

This assumption is important because by having the bacteria growing in this region, degrading the contaminant, concentration gradients are increased (Seagren et al., 1993). These increased gradients cause the contaminant to dissolve faster, speeding up remediation.

In this paper, a new method of bacteria visualization is discussed. This new method will validate of this assumption. A new technique needed to be developed because of limitations in previous methods.

Previous Methods

The earliest techniques used to look at bacteria in a flow system used flow cells (Caldwell and Lawrence, 1988). These flow cells are generally two cover slips separated by the distance of a microscope slide wherein the water and bacteria flow. These flow cells allowed the visualization of bacterial attachment and detachment in a flowing environment. However, since the bacteria weren't in a matrix with some tortuosity, the

behavior viewed applied better to bacteria near a surface in a river or lake than to bacteria in the subsurface.

Micromodels were employed to better simulate a porous medium (Wan et al., 1994). Bacteria could be viewed using the micromodel under a microscope. Since a micromodel is 1/4" thick, objectives using a coverslip correction had to be used. This meant that magnification was limited.

Although bacteria could be seen in a micromodel using a standard microscope, the use of this method was limited. In order to see unstained bacteria, the greatest magnification possible was used. This limited the field of view to just a few pores. A further limit on the usefulness of microscopy was imposed by the micromodel itself.

Because a micromodel's pores have a certain depth and curves on the sides, focusing on the bacteria was difficult. If the microscope was focused on one plane in the pore, bacteria in another plane might be missed. The curved sides also meant that bacteria in the sides of the pores were difficult to see and often missed.

The bacteria also were difficult to distinguish from structures in the micromodel. This was especially true in darkfield microscopy. Using darkfield microscopy, the bacteria show as white points. Blemishes in the glass used for making the micromodels also show up as white points, and it is up to the viewer to be able to distinguish between the two. When the model is under flow conditions and being viewed in real-time, it is easy to do. However with photographs or static conditions, this task becomes much more difficult.

Because of these limits, fluorescence microscopy was employed. This allowed bacteria at the sides of pore throats to be seen, as well as allowing a larger field of view. With fluorescent microscopy came the problem of finding either fluorescent bacteria or a useful stain. Because of how the experiment this method was to be used with was envisioned, several constraints were placed on stain selection.

In order to use fluorescent microscopy to see where the bacteria colonized in a contaminant plume, the stain had to leave the bacteria alive. The stain also had to be taken up intracellularly. This is because surface stains, which change the surface chemistry of the bacterial, could also change the cell's attachment and detachment behavior. In order to see their colonization bacteria, the stain also had to be long lasting.

There were also limits inherent to microscopy. Most microscope stages are horizontal and I wanted to run my experiment vertically to better simulate the subsurface. Although a cradle can be built for the microscope and then used so that the micromodel is run vertical, this is not optimum. Another problem is the size of the objectives. Because the objectives are so large, they limit where one can look on the micromodel. If the plumbing inlets and outlets are simple, limited and far apart, essentially the entire model can be viewed. Since I needed to have inlets and outlets for water and bacteria as well as for the contaminant reservoir and valves to control flow, this didn't allow me to view the entire model. I could only see over a very limited range of the model.

I also couldn't use autoclavable teflon tubing because the technique used previously to hold the tubing in place employed epoxy which wouldn't work with teflon. I could have used other types of tubing but wished to use teflon because of its flexibility and transparency. The transparency was important so that I could see where air bubbles were in the tubing and prevent them from entering the model. Because of this limitation I had to go back to earlier methods involving clamps. This would raise the micromodel off the stage of the microscope. These clamps are 1/4" thick on each side of the model and would limit my ability to focus by lowering the focusing range. These clamps, because they are large, would also impose further limits on the size of the visualization field.

New Method

The new method employs principles of fluorescent microscopy while not using a microscope. The theory is that light from a light source will pass through band pass

filters, limiting the light's wavelengths. This light will then be dispersed by a concave filter and pass through the micromodel. The fluorescent chemicals or particles in the micromodel will then absorb the light and emit a higher wavelength. These two wavelengths are then transmitted to a post-filter that cuts off the lower wavelength.

The bacteria were made fluorescent by the use of CellTracker fluorescent probes (Molecular Probes). CellTracker is a line of stains that are retained in living cells through several generations. They pass freely through cell membranes, but once inside the cell, undergo a reaction producing a cell-impermeant reaction product.

All of the CellTracker dyes contain a chloromethyl reactive group. The reaction is believed to be a glutathione S-transferase-mediated reaction (Molecular Probes, 1992). This reaction has been shown to occur *in vitro.*

After receiving the stains, a 10 mM solution was made in dimethylsulfoxide (DMSO). Prior to loading the stains, the cells were centrifuged at 12,100 x g for 10 minutes and the supernatant was then removed. The cells were then resuspended in a 25 mM solution of stain in mineral medium. They were then incubated for 45 minutes and recentrifuged. The cells were resuspended in sterile mineral medium and incubated for at least 30 minutes. After this last incubation the cells were washed again and resuspended in mineral medium for use in the experiment.

We used five probes, to determine the optimal stain and filter combination for visualization.

The filters were purchased from Oriel Corp. (Stratford, CT) and Andover Corp. (Salem, NH). Andover Corp. supplied all of the post-filters. The pre-filters are 2" round. The post-filters are 6.5" Schott glass squares to allow the viewing apparatus to move around the model without having to move the filter. A concave filter to spread the light after the pre-filter was purchased from Melles-Griot (Irvine, CA).

CellTracker Probe	λEX (nm)	λEM (nm)	pre-filter	post-filter
Blue CMAC	354	469	Hoya Glass U-330†	GG-420
Blue CMHC	372	470	Hoya Glass U-330†	GG-420
Green CMFDA	490	520	500 nm cutoff*	OG-515
Orange CMTMR	541	565	540+/- 5 nm bandpass†	OG-550
Yellow-Green CMEDA	522	543	520+/- 5 nm bandpass†	OG-530

Table 1 List of probes used, their fluorescence excitation (λEX) and emission (λEM) maxima and filter combination used. * indicates filters purchased through Andover, † indicates filters purchased through Oriel Corp.

The filters are held in filter holders installed in a wooden box built at New Mexico Tech by Paul Hofmann. The pre-filters are inside the box. The micromodel is also located inside the box, at the other side. Tubing is connected to the micromodel using c-clamps with Swagelok VCO fittings. The tubing runs from the micromodel through holes in the box to syringe pumps (for inlets) or flasks (for outlets). The post-filter is held to the outside of the box also using c-clamps with VCO fittings.

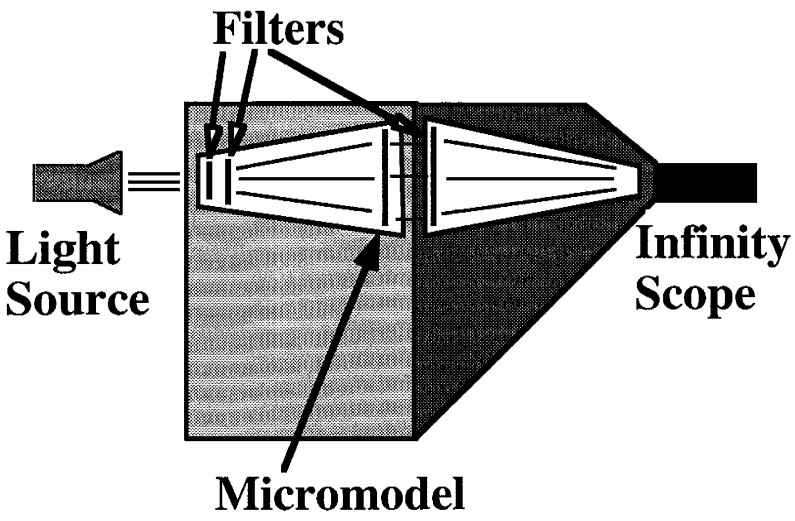

Figure 1 Filter box schematic

The Infinity Scope is a microscope that consists of a series of tubes and lenses. It allows magnification of 2.2x to 52.5x using eyepieces. Photographic images would have a magnification range of 1/2 that. Video magnification ranges from 83.6x to 1995x. Because of the low light conditions, an ultra low-light black and white CCD camera (Richter Enterprises, model CMC-1) and a high sensitivity color camera (Cohu Enterprises, model 8215) were used.

Results

Using a fluorescent microscope, the blue stains are the brightest and most distinguishable from model imperfections.

The green and yellow-green stains work best in the filter box using the ultra low-light camera. This is due to light leakage. The green and yellow-green stains undergo transformations intracellularly to fluoroscein. The filter set-up for fluoroscein was the set-up with the most light leakage. This was because fluoroscein has no particular chemical structure and so its absorbance and emission wavelengths are very wide to allow for the different structures. Since this is the case, not using stains at all would be best. The black and white camera also had problems distinguishing grays and was of low resolution.

For the color camera, the blue stains were used. They worked okay. They actually worked better for low concentrations when the post-filter was removed and the pre-filter was replaced by the 500 nm cutoff filter. This was because the few bacteria could not supply enough light to make the camera pick up them. They did provide enough light to make them distinguishable, by color, from the background light. Higher concentrations of bacteria allowed the standard set-up to be used.

The orange stain did not work well at all. There was a red precipitate associated with the stain, using the standard procedure. They also didn't appear to fluoresce at the stated wavelength, even under the microscope. It did appear that they fluoresced slightly using fluoroscein wavelengths.

I feel that this method would be improved with a better light source. The current light source is not optically adequate. I think a better method for holding the filters and model should be devised. A box was used originally to keep the experiment in the dark. If a dark room could be set-up with a vibration free table with a bread board top, this would be optimum. Standard filter holders could then be used and would be better aligned.

References

Caldwell, D.E., and J.R. Lawrence. 1988. Study of Attached Cells in Continuous-Flow Slide Culture. in CRC Handbook of Laboratory Model Systems for Microbial Ecosystems, Vol. 1. J.W.T. Wimpenny, Ed. pp 117-138.

Davis, J.W., N.J. Klier, C.L. Carpenter. 1994. Natural Biological Attenuation of Benzene in Ground Water Beneath a Manufacturing Facility. Ground Water. 32:215-226.

Molecular Probes. Dec. 30, 1992. CellTracker™ New Fluorescent Probes for Long-Term Tracing of Living Cells. MP bulletin 2925.

Seagren, E.A., B.E. Rittmann, A.J. Valocchi. 1993. Quantitative Evaluation of Flushing and Biodegradation for Enhancing in situ Dissolution of Nonaqueous-phase Liquids. J. Cont. Hyd. 12:103-132.

Wan, J., J.L. Wilson, and T.L. Kieft. 1994. Influence of the Gas-Water Interface on Transport of Microorganisms through Unsaturated Porous Media. Applied and Env. Micro. 60:509-516.

2. Dissolution of Fluids from Reservoir in a Micromodel

Introduction

Solute concentration profiles for the aqueous phase in subsurface systems are highly dependent on flow rates and contaminant saturations (Miller et al., 1990). Among the characteristics of contaminant saturation that are important are blob shape and size and lateral dimensions of the exposure zone (Powers et al., 1991). In order to simulate a contaminant dissolution experiment conducted in a column, a micromodel pattern that mimicked the contaminant saturation characteristics were designed.

A series of experiments was then carried out in order to determine which flow rate to use in this micromodel experiment. Since the micromodel does not translate directly one to one to the column experiment, the flow rate that was used in the column experiment could not be used. Another one had to be established either mathematically or experimentally.

Mathematically it is very difficult to scale flow rates from three dimensional columns to two dimensional micromodels. Scaling from one dimension to three dimensions presents a problem than can be solved mathematically. To translate from two dimensions to three is much more difficult. Mathematically, it is easier to translate from odd to odd dimensions rather going from odd to even.

Another problem I encountered in this translation is the definition of micromodel porosity. Because of their unique quality's, a micromodel's porosity is hard to define. They are porous because they allow fluid flow. It is difficult to measure this porosity because it is hard to measure the volume the two dimensional network occupies. The definition of how much of the glass the network occupies is difficult to answer, should the measurement of porosity be based on the entire model, or just the area the pattern occupies? Should the whole thickness of the glass be included or just the thickness the pores occupy?

Because of these difficulties, an experimental approach was chosen. It was decided that the flow rate that produced a plume that extended 1/2 to 3/4 of the way down the model would be used.

A plume that extended to the bottom of the model would not allow for the bacteria to colonize on the edges. A plume that did not extend far enough would not allow for a wide sufficient breadth of contaminant concentrations.

Methods

Fluoroscein (Uranine, Fisher Scientific) was used as an indicator of plume depth. Using various concentrations of fluoroscein in water and flow rates, a plume depth was determined. The water was emplaced into the reservoir where the toluene would go. The high concentration used was 500 mg/L. At this concentration, the plume was most easily visible.

Tests were also made with toluene in the reservoir. Fluoroscein is a sodium salt soluble in water. It is not soluble in organics. A mixture of toluene and DMSO was used in order to obtain a semi-stable suspension of fluoroscein in the organic phase. In toluene, fluoroscein does not fluoresce. It does partition out of the toluene into the water where it does fluoresce. The actual toluene plume had to be viewed in the filter box due to the low resultant fluoroscein concentrations in the aqueous phase.

The filter box is a wooden box which holds a series of filters and the micromodel. The first set of filters narrows the wavelength of light transmitted to the micromodel. Fluorescent particles or chemicals in the micromodel can then absorb this wavelength and emit a higher wavelength of light. A second filter then cuts off the lower, absorbing wavelength so that only the emitted light passes through. Fluoroscein absorbs light in the 480-510 nm region and emits above 520.

0.05 ml of toluene was sampled for in the effluent using a teflon sampling valve. The pore volume of the micromodel is 0.1 ml. By weighing the micromodel before and

after filling the model with water, the pore volume was determined. By measuring the volume of the reservoirs independently, the actual volume in the pattern could be determined.

The toluene was dripped into a sample vial containing 1 ml of methylene chloride. A gas chromatograph was then used to determine toluene concentrations. Because of the low sampling volumes, the methylene chloride was used to capture all of the toluene and limit volatilization.

Results

The aqueous solution of fluoroscein yielded a visible plume, up to ~1/4 of the way down the model. However, the reservoir was designed to have an organic liquid in the reservoir and to trap the fluid in the reservoir by capillary forces. Since the fluoroscein solution was aqueous, no capillary forces were involved. The water flowing in the main body of the model took a shortcut through the reservoir. This was because the reservoir had much less resistivity to flow than the pattern. The plume that was obtained was then just a trace of the flow paths through the reservoir.

The fluoroscein/toluene mix suspension showed that capillary forces do indeed trap the blob in the reservoir and don't allow for shortcuts through the reservoir. Because the concentrations achieved were much lower than the aqueous solution's, the visibility of the plume was hampered. It appears that 0.05 ml/hr is the optimum flow rate -- it gets to 3/4 of the way down the model.

A flow rate of 0.05 ml/hr is equivalent to 1/2 pore volumes/hr or 24.4 cm/hr. The flow rate used in Illinois was 1/10 pore volume/hr.

References

Miller, C.T., M.M. Poirier-McNeill, and A.S. Mayer. 1990. Dissolution of Trapped Nonaqueous Phase Liquids: Mass Transfer Characteristics. WRR. 26:2783-2796.

Powers, S.E., C.O. Loureiro, L.M. Abriola, and W.J. Weber, Jr. 1991. Theoretical Study of the Significance of Nonequilibrium Dissolution of Nonaqueous Phase Liquids in Subsurface Systems. WRR. 27: 463-477.

D. Appendix D: Experimental Data

1. Model 1 data

Experiment D1

Δ time (h)	cumulative time	reading	mass (mg)	cumulative mass (mg)	comments
1	1	0	0.000	0.000	*
1	2	49138	0.019	0.019	
1	3	18369	0.007	0.026	
1.5	4.5	2350664	0.908	0.934	*
1.5	6	9640	0.004	0.938	
1	7	41710	0.016	0.954	
1	8	12460	0.005	0.958	*
3.17	11.17	4994	0.002	0.960	
1.33	12.5	792	0.000	0.961	
14.5	27	1701499	0.657	1.618	
4	31	455898	0.176	1.794	
2	33	4374	0.002	1.796	
17.33	50.33	0	0.000	1.796	*
3	53.33	636	0.000	1.796	
1.67	55	2794	0.001	1.797	
13.5	68.5	15868	0.006	1.803	*
2.75	71.25	103311	0.040	1.843	
5	76.25	211001	0.081	1.924	
*=volatilization problems					
standard (100 mg/l) = 261538					
run April 9 to April 12					

Experiment C1

Δ time (h)	cumulative time	reading	mass (mg)	cumulative mass (mg)	comments
3	3	11103	0.004	0.004	*
4.83	7.83	5350	0.002	0.006	*
11.17	19	0	0.000	0.006	*
4	23	0	0.000	0.006	*
2	25	624160	0.241	0.247	
2.1	27.1	9824	0.004	0.251	
2.07	29.17	175005	0.068	0.319	
2.08	31.25	0	0.000	0.319	*
10.5	41.75	1769703	0.683	1.002	
6.75	48.5	0	0.000	1.002	*
3	51.5	1210	0.000	1.003	*
2	53.5	0	0.000	1.003	*
18.67	72.17	215658	0.083	1.086	
*=volatilization problems					
standard (100 mg/l) = 261538					
run April 14 to April 17					

Experiment B1

Δ time (h)	cumulative time	reading	mass (mg)	cumulative mass (mg)	comments
2.1	2.1	0	0.0000	0.000	
3.33	5.43	2659	0.0004	0.000	
2.15	7.58	2309	0.0003	0.001	
9.45	17.03	3102	0.0005	0.001	
5.67	22.7	1262	0.0002	0.001	
2.75	25.45	1451	0.0002	0.002	
2.55	28	0	0.0000	0.002	
2.08	30.08	1320	0.0002	0.002	
12.25	42.33	1659	0.0002	0.002	
1.67	44	1170	0.0002	0.002	
2	46	1895	0.0003	0.002	
2.5	48.5	1452	0.0002	0.003	
1.75	50.25	1768	0.0003	0.003	
1.75	52	1685	0.0002	0.003	
2	54	885	0.0001	0.003	
2	56	1026	0.0002	0.003	
10.33	66.33	4514	0.0007	0.004	
2.67	69	1919	0.0003	0.004	
1.5	70.5	1650	0.0002	0.005	
1.5	72	0	0.0000	0.005	
*=volatilization problems					
standard (100 mg/l) = 687481					
run May 8 to May 11					

2. Model 2 data

Experiment D2

Δ time (h)	cumulative time	reading	mass (mg)	cumulative mass (mg)	comments
16.25	16.25	2268438	0.876	0.876	*
2.17	18.42	187124	0.072	0.948	
2	20.42	3714	0.001	0.950	*
1.58	22	9368	0.004	0.953	
2	24	847	0.000	0.954	*
1.75	25.75	374355	0.145	1.098	
11.17	36.92	3295	0.001	1.100	
2.33	39.25	1866	0.001	1.100	*
1.75	41	0	0.000	1.100	*
2	43	0	0.000	1.100	*
2.25	45.25	0	0.000	1.100	*
1.75	47	0	0.000	1.100	
1.92	48.92	0	0.000	1.100	*
11.58	60.5	0	0.000	1.100	*
*=volatilization problems					
standard (100 mg/l) = 261538					
run April 17 to April 20					

Experiment C2

Δ time (h)	cumulative time	reading	mass (mg)	cumulative mass (mg)	comments
2	2	9258	0.001	0.001	
2.07	4.07	0	0.000	0.001	
1.53	5.6	0	0.000	0.001	
2	7.6	0	0.000	0.001	
12.33	19.93	2620	0.000	0.002	
1.75	21.68	19886	0.003	0.005	
1.92	23.6	1632	0.000	0.005	
2.33	25.93	1697	0.000	0.005	
1.75	27.68	6132	0.001	0.006	
1.95	29.63	1343	0.000	0.006	
1.94	31.57	2007	0.000	0.007	
12.16	43.73	4764	0.001	0.007	
1.94	45.67	17885	0.003	0.010	
1.93	47.6	1440	0.000	0.010	
2	49.6	253244	0.038	0.048	
2	51.6	9308	0.001	0.050	
2	53.6	1468	0.000	0.050	
13.94	67.54	276358	0.041	0.091	
2.15	69.69	1374	0.000	0.091	
1.51	71.2	1256	0.000	0.092	
*=volatilization problems					
standard (100 mg/l) = 675111					
run April 26 to April 29					

Experiment B2

Δ time (h)	cumulative time	reading	mass (mg)	cumulative mass (mg)	comments
2	2	84872	0.012	0.012	
3	5	67239	0.009	0.021	
7.25	12.25	30622	0.004	0.026	
9	21.25	39922	0.006	0.031	
3.95	25.2	15497	0.002	0.033	
1.8	27	26643	0.004	0.037	
2.05	29.05	22290	0.003	0.040	
18.02	47.07	921876	0.129	0.169	
1.93	49	14171	0.002	0.171	
2.05	51.05	41287	0.006	0.177	
2.95	54	5351	0.001	0.178	
2.05	56.05	0	0.000	0.178	
12.03	68.08	0	0.000	0.178	
2.17	70.25	9948	0.001	0.179	
1.9	72.15	249701	0.035	0.214	
*=volatilization problems					
standard (100 mg/l) = 721200					
run May 13 to May 16					
there were alot of toluene blobs outside of the reservoir					

3. Model 3 data

Experiment D3

Δ time (h)	cumulative time	reading	mass (mg)	cumulative mass (mg)	comments
2.2	2.2	2771278	0.421	0.421	
2	4.2	92585	0.014	0.435	
1.8	6	0	0.000	0.435	*
2	8	689930	0.105	0.540	
14.33	22.33	239256	0.036	0.576	
3.67	26	195557	0.030	0.606	
4	30	1866	0.000	0.606	
3.15	33.15	187594	0.029	0.635	
19.1	52.25	637997	0.097	0.732	
1.75	54	356108	0.054	0.786	
3.25	57.25	206167	0.031	0.817	*
2.3	59.55	60600	0.009	0.827	
9.5	69.05	252251	0.038	0.865	
*=volatilization problems					
standard (100 mg/l) = 664627					
run May 6 to May 9					

Experiment C3

Δ time (h)	cumulative time	reading	mass (mg)	cumulative mass (mg)	comments
2	2	2271018	0.319	0.319	
2	4	2261950	0.318	0.636	
2.25	6.25	3399362	0.477	1.114	
1.67	7.92	47276	0.007	1.120	
3.08	11	3219101	0.452	1.572	*
13.2	24.2	4617805	0.648	2.221	
1.8	26	40278	0.006	2.226	
2.5	28.5	1055269	0.148	2.374	
1.85	30.35	472546	0.066	2.441	
1.65	32	2218	0.000	2.441	
1.95	33.95	151820	0.021	2.462	
2	35.95	3708	0.001	2.463	
14.2	50.15	3085	0.000	2.463	
1.75	51.9	6499	0.001	2.464	
2	53.9	18416	0.003	2.467	
3	56.9	385889	0.054	2.521	
7.25	64.15	3157	0.000	2.521	
9	73.15	190243	0.027	2.548	
*=volatilization problems					
standard (100 mg/l) = 719404					
run May 11 to May 14					

Experiment B3

Δ time (h)	cumulative time	reading	mass (mg)	cumulative mass (mg)	comments
1.95	1.95	765670	0.124	0.124	
10.86	12.81	2198752	0.355	0.479	
2.79	15.6	7316	0.001	0.480	
1.4	17	753671	0.122	0.601	
2.5	19.5	475608	0.077	0.678	
2.55	22.05	313002	0.051	0.729	
2.15	24.2	781811	0.126	0.855	
1.95	26.15	861398	0.139	0.994	
10.85	37	392343	0.063	1.057	
2	39	187167	0.030	1.088	
1.95	40.95	2977	0.000	1.088	
2.05	43	1685	0.000	1.088	
18.5	61.5	49049	0.008	1.096	
2.5	64	4620	0.001	1.097	
2.05	66.05	7018	0.001	1.098	
2.1	68.15	1089	0.000	1.098	
1.9	70.05	16961	0.003	1.101	
2.04	72.09	2670	0.000	1.101	
*=volatilization problems					
standard (100 mg/l) = 625647					
run May 17 to May 20					

4. Room Temperature Data

Data from May 9, 1994, through May 20 for MSEC 151 (dates bacterial experiments were run). Data from May 8 is missing due to computer data loss.

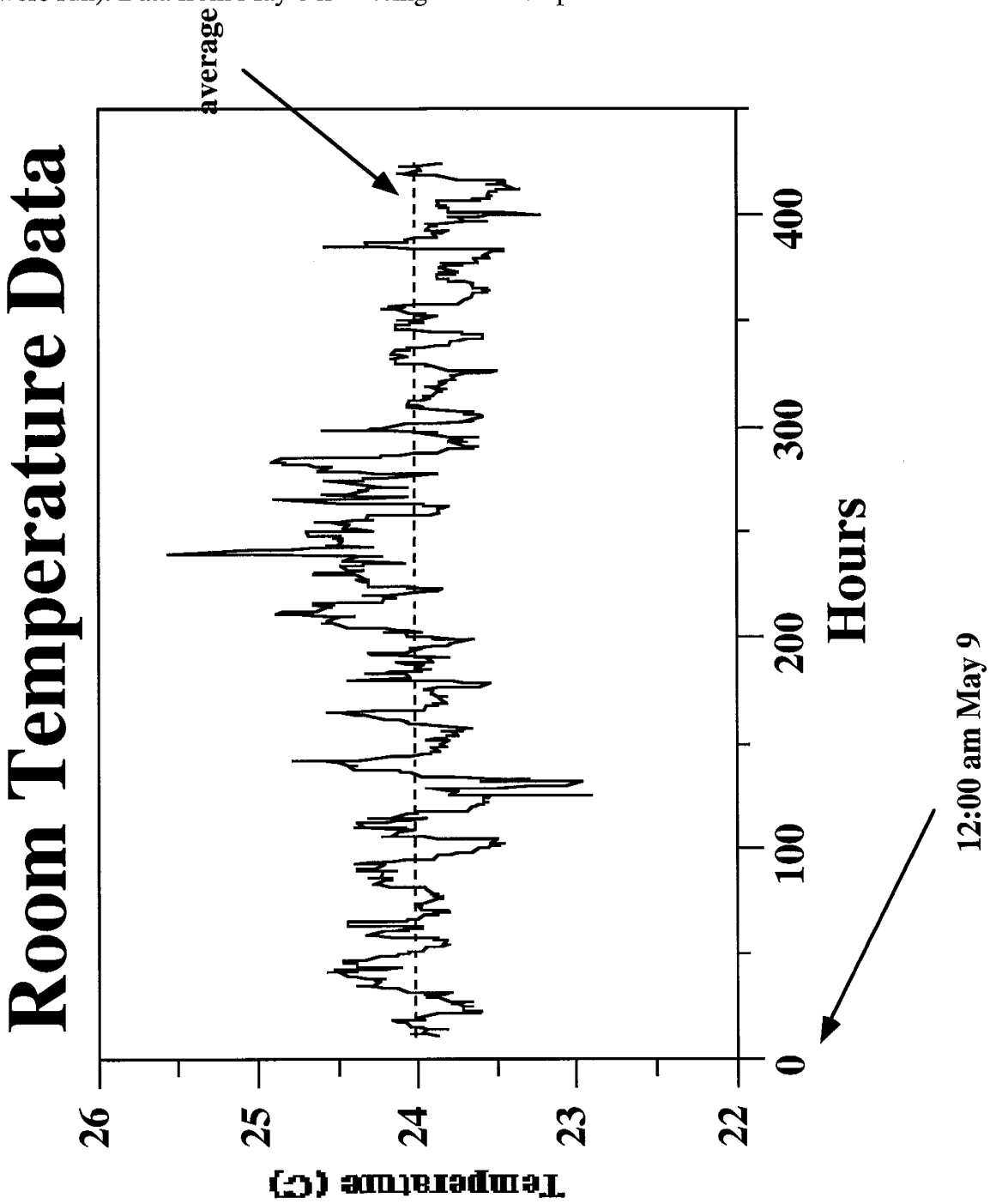

5. Percentage of Pore Covered by Bacteria

This percentage was arrived at by observation of pores in the indicated areas. All percentages are approximate. The percentages were determined in increments of 5, the averages are in increments of 0.5.

	0h		24h		48h		72h	
Area	ave.	no. of pores*	ave.	no. of pores	ave.	no. of pores	ave.	no. of pores
I	1.5	15	2.5	18	3.5	21	5.0	18
II	0.5	16	1.0	26	0.5	19	0.0	18
III	0.0	24	0.5	22	0.5	18	1.0	9
A	2.5	10	4.0	16	5.0	14	9.0	12

*no. of pores refers to the number of pores observed that went into the average for that area and time. This amount varies because the number of pores videotaped in an area for a given time varies.